UC Irvine
UC Irvine Previously Published Works

Title

The Fundamental Physics of Directive Beaming at Microwave and Optical Frequencies and the Role of Leaky Waves

Permalink

https://escholarship.org/uc/item/0h95v3vb

Journal

Proceedings of the IEEE, 99(10)

ISSN

0018-9219

Authors

Jackson, David R
Burghignoli, Paolo
Lovat, Giampiero
et al.

Publication Date

2011-10-01

DOI

10.1109/jproc.2010.2103530

The Fundamental Physics of Directive Beaming at Microwave and Optical Frequencies and the Role of Leaky Waves

Directive beaming through periodic structures at microwave and optical frequencies are discussed in this paper, as is the role of weakly-attenuated leaky waves in these structures.

By David R. Jackson, *Fellow IEEE*, Paolo Burghignoli, *Senior Member IEEE*,
Giampiero Lovat, *Member IEEE*, Filippo Capolino, *Senior Member IEEE*,
Ji Chen, Donald R. Wilton, *Life Fellow IEEE*, and Arthur A. Oliner, *Fellow IEEE*

ABSTRACT | This review paper summarizes various aspects of directive beaming and explains these aspects in terms of leaky waves. Directive beaming occurs in antenna design where a narrow beam is obtainable by using fairly simple planar structures excited by a single source. These structures include Fabry–Pérot cavity structures as well as metamaterial structures made from artificial low-permittivity media. Directive beaming also occurs in the optical area where it has been observed that highly directive beams can be produced from small apertures in a metal film when an appropriate periodic patterning is placed on the film. One aspect that these phenomena all have in common is that they are due to the excitation of one or more weakly attenuated leaky waves, the radiation from which forms the directive beam. This is established in each case by examining the role of the leaky waves in determining the near-field on the aperture of the structure and the far-field radiation pattern of the structure.

KEYWORDS | Directive beaming; electromagnetic bandgap (EBG) antenna; enhanced transmission; Fabry–Pérot cavity; leaky-wave antenna; metamaterial; plasmon

D. R. Jackson, **J. Chen**, and **D. R. Wilton** are with the Department of Electrical and Computer Engineering, University of Houston, Houston, TX 77204-4005 USA (e-mail: djackson@uh.edu; jchen18@uh.edu; wilton@uh.edu).
P. Burghignoli is with the Department of Information Engineering, Electronics and Telecommunications, "La Sapienza" University of Rome, 00184 Rome, Italy (e-mail: burghignoli@die.uniroma1.it).
G. Lovat is with the Department of Astronautical, Electrical, and Energetic Engineering, "La Sapienza" University of Rome, 00184 Rome, Italy (e-mail: giampiero.lovat@uniroma1.it).
F. Capolino is with the Department of Electrical Engineering and Computer Science, University of California, Irvine, Irvine, CA 92697-2625 USA (e-mail: f.capolino@uci.edu).
A. A. Oliner is with the Department of Electrical Engineering, Polytechnic University, Brooklyn, NY 11201 USA (e-mail: aaoliner@gmail.com).

I. INTRODUCTION

The subject of directive beaming from planar structures that are excited by a simple source is one that has had a fairly rich and interesting history, extending from the 1950s until the present time. Interesting applications of directive beaming include the construction of novel highly directive antennas as well as interesting optical effects such as the narrow beaming of light from a subwavelength aperture, and a related effect, the enhanced transmission of light through a subwavelength aperture. The purpose of this review paper is to overview directive beaming in both microwaves and optics, and to give a unified discussion of the directive-beaming phenomenon from the point of view of leaky waves (also called leaky modes; the two terms are

used interchangeably here, though "mode" is used to emphasize the modal aspect of the wave). In all cases, it is seen that leaky waves play a key role in explaining the phenomena. Leaky-wave theory also allows for simple design formulas that can be used to optimize the designs.

In the area of antennas, directive beaming was first examined by von Trentini [1] who used a parallel-plate cavity formed by a ground plane on the bottom and a partially reflecting surface (PRS) on the top. The PRS consisted of a 2-D array of metal patches, or a 2-D array of slots in the top plate, or a 1-D array of metal wires. The structure was excited by a simple source such as a centrally located slot on the ground plane that was fed by a waveguide. It was observed that highly directive beams could be produced if the thickness of the parallel-plate region was chosen appropriately, and simple design equations for predicting the optimum thickness were given.

Later, directive beaming was observed from similar structures using various types of PRS covers. In [2] and [3], a high-permittivity dielectric superstrate was used, and the parallel-plate region was allowed to be dielectric filled, resulting in a dielectric "substrate/superstrate" structure. This structure demonstrated narrow pencil beams at broadside or narrow conical beams where the radiation is focused at a scan angle θ_0 from the vertical axis. Using multiple superstate layers allowed for a further increase in the directivity of the antenna [4]–[6].

An improved version of the von Trentini structure was presented in [7], where it was also noted that this type of antenna is similar to the Fabry–Pérot interferometer cavity, with one side of the cavity being a perfectly reflecting ground plane. Hence, these PRS antennas are often referred to as "Fabry–Pérot cavity antennas." In [7], Feresidis and Vardaxoglou make the interesting note that this type of antenna would have a greater bandwidth if the phase of its PRS were to linearly increase with frequency so that the phase variation of the PRS would compensate for the frequency variation of the cavity. They investigated PRSs made from several different types of elements, including crossed dipoles, patches, rings, and square loops. They found that the dipole elements, or square or circular patch elements (or their complementary structures), produced less of a variation of the beam with frequency, especially with close packing of the elements in the periodic PRS array.

PRS structures involving planar 2-D periodic arrays of metal patches or slots in a conducting plate of various configurations were then analyzed [7]–[12], and the radiation characteristics were examined in detail. An analysis was then presented in [13] that was more general, and showed the basic radiation characteristics of any PRS-based Fabry–Pérot cavity type of antenna.

All of the above structures fall into the general category of what is called here a PRS antenna, whose general configuration is shown in Fig. 1. The structure consists of a grounded substrate of thickness h having material param-
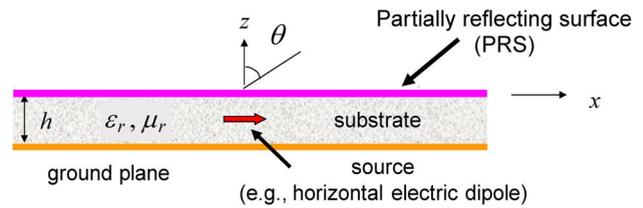

Fig. 1. *A leaky-wave antenna made from a PRS over a grounded substrate layer. The structure is excited by a simple source (such as a horizontal electric dipole) inside the substrate.*

eters ε_r, μ_r, on top of which is placed the PRS. The structure is excited by a simple source inside the substrate, which is shown in Fig. 1 as a horizontal electric dipole in the middle of the substrate, though other sources can be used. This structure has appeared in the literature under various names, including "cavity reflex antenna," "Fabry–Pérot cavity antenna," "electromagnetic bandgap (EBG) antenna," "planar leaky-wave antenna," and variants of these names. (The term "EBG" arises from the consideration that the PRS may consist of a stack of dielectric layers or other elements, forming an EBG structure [14]–[16].) One of the purposes of this paper is to review the general properties of such structures, and to explain how they operate as leaky-wave antennas. In particular, the PRS acts as a "metasurface" as seen by the waves inside the substrate, to confine the power that flows outward from the source in the form of radially propagating leaky waves, whose properties determine the nature of the radiation pattern. (The leaky waves will be radially propagating provided the source is of finite extent, such as a dipole. A uniform line source will excite a pair of leaky waves propagating linearly outward from the source.)

A second type of structure that was recently developed for directive beaming is the metamaterial wire-medium slab structure, consisting of an artificial low-permittivity slab composed of a periodic array of conducting wires placed over a ground plane [17]–[19] as shown in Fig. 2.
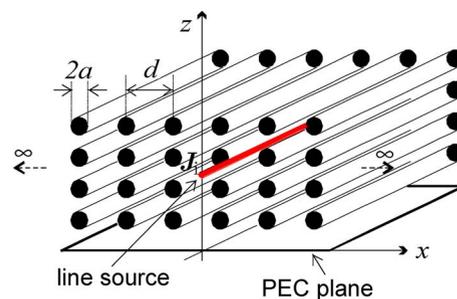

Fig. 2. *A highly directive antenna consisting of a metamaterial slab of artificial material (wire medium) having a low permittivity. The structure is excited by a line source inside the artificial slab. (Figure is adapted from [34].)*
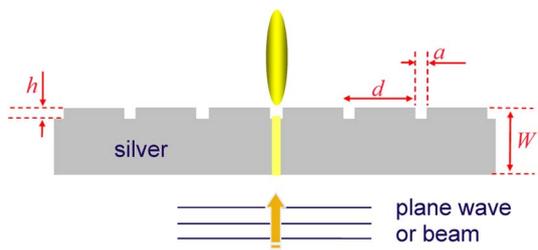
Fig. 3. *Illustration of the directive beaming effect at optical frequencies. A plane wave incident on a silver film that has a hole in it. The exit face of the film has a periodic array of grooves. (Figure is adapted from [59].)*

The structure is excited by a simple source inside the artificial slab such as a dipole or a uniform line source (a line source is shown in Fig. 2). Directive beams are obtained when the effective permittivity of the substrate is small compared to that of the surrounding air, especially when the thickness of the wire medium slab is optimized. This phenomenon is reviewed here and an explanation in terms of leaky waves is given.

A third interesting phenomenon discussed here is the directive beaming of light from a subwavelength aperture in a metal film such as silver or gold (that exhibits plasmonic properties at optical frequencies), when the film is properly patterned using a periodic structure. A typical structure is shown in Fig. 3, in which a beam of light impinges on a silver film, and excites an aperture on the opposite (exit) side, which has a periodic set of grooves. This phenomenon is investigated here and it is established that the beaming is due to the excitation of a leaky wave, though in this case the structure is acting as a periodic type of leaky-wave antenna where radiation occurs via a higher order space harmonic, as opposed to a uniform or quasi-uniform type of leaky-wave antenna, where radiation occurs from the fundamental space harmonic (as for the structures of Figs. 1 and 2).

II. ANTENNAS BASED ON A PRS

A. Introduction

The general PRS antenna is shown in Fig. 1. A grounded substrate has a planar PRS structure on top, and is excited by a simple source inside the substrate. The bottom ground plane and the top PRS cover form a parallel-plate region, which for analysis purposes is assumed to be infinite in the horizontal (x, y)-directions, though in practice it would be finite in size and possibly terminated with absorber at the perimeter of the structure. The substrate of thickness h has, in general, material parameters ε_r, μ_r, though the substrate could also be air (the pros and cons of using an air substrate are discussed later in Sections II-E–G). The structure is usually excited by a

single source inside the parallel-plate region that is centrally located horizontally. A practical source (or feed) might be a waveguide-fed slot on the ground plane, a patch antenna placed on the ground plane, or a wire antenna that is excited from below the ground plane. The shape of the radiation pattern is primarily determined by the substrate and PRS properties, and only to a minor degree by the type of source. However, the type and location of the source will strongly influence the level of the radiation from the structure, and hence have a significant effect on the input resistance or conductance seen at the feed terminals. Also, as discussed immediately below, vertical dipole sources cannot be used to produce a broadside beam, but only a conical beam.

For the purposes of modeling the radiation pattern, a simple source such as an electric or a magnetic dipole is commonly used. Fig. 1 shows a horizontal electric dipole (HED) placed in the middle of the cavity vertically. Such a source can be used to produce either a pencil beam at broadside or a conical beam focused at a scan angle θ_0, as shown in Fig. 4(a) and (b), respectively. The vertical placement of the dipole source does not significantly affect the beam shape, but it does directly affect the power radiated by the source, which in turn directly influences the input resistance seen by a practical feed. Placing the HED source in the middle of the substrate maximizes the power radiated by the source, since the horizontal electric field of the leaky mode (leaky parallel-plate mode) is maximum there (as discussed in Section II-B), and hence the HED source couples the strongest with the leaky mode when located there. Another source that can be used is the horizontal magnetic dipole (HMD) source. In this case, the
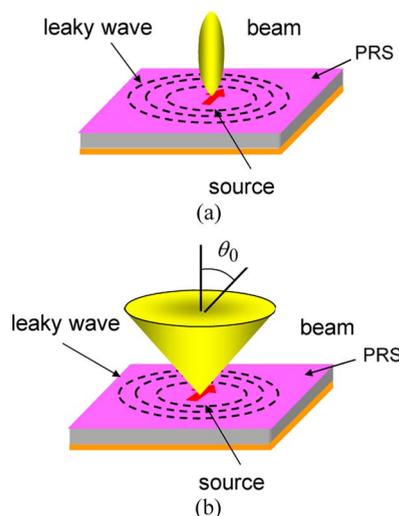

Fig. 4. *Illustration of the two types of radiation patterns that can be obtained from the PRS structure of Fig. 1. (a) A symmetric pencil beam at broadside. (b) A conical beam at a scan angle θ_0. The radially propagating leaky mode is also illustrated. (Figure is adapted from [62].)*

radiated power is maximized when the source is placed on the ground plane. Assuming that the HED is oriented in the x-direction or the HMD is oriented in the y-direction, the xz-plane ($\phi = 0$) is the E-plane of the antenna where the radiated field has mainly an E_θ component, and the yz-plane ($\phi = 90°$) is the H-plane having mainly an E_ϕ component. A vertical electric dipole (VED) or vertical magnetic dipole (VMD) source can only be used to produce a conical beam as shown in Fig. 4(b). In this case, the pattern is omnidirectional in azimuth, and polarized with E_θ or E_ϕ, respectively. Maximum power is radiated when the VED is on the ground plane and the VMD is placed in the middle of the substrate vertically.

Various types of PRS surfaces have been investigated in the past. Examples are shown in Fig. 5, which shows an HED in the x-direction as the source. Fig. 5(a) shows a stack of one or more high-permittivity superstrate layers placed on top of the substrate. Fig. 5(b) shows a PRS composed of a planar 2-D periodic array of metal patches (or dipoles). The metal patches are assumed to have a length L in the x-direction and width W in the y-direction, with periodic spacings a in the x-direction and b in the y-direction. Fig. 5(c) shows the complementary structure, consisting of a periodic array of rectangular slots in a conducting plate, having length L in the y-direction and W in the x-direction, with periodic spacings a and b in the y- and x-directions, respectively. (The slots are rotated $90°$ from the corresponding patches for convenience, so that the E- and H-planes continue to be the same.) Fig. 5(d) shows a PRS made from a 1-D periodic arrangement of conducting wires or metallic strips, with metallic strips allowing for a printed-circuit realization of the PRS
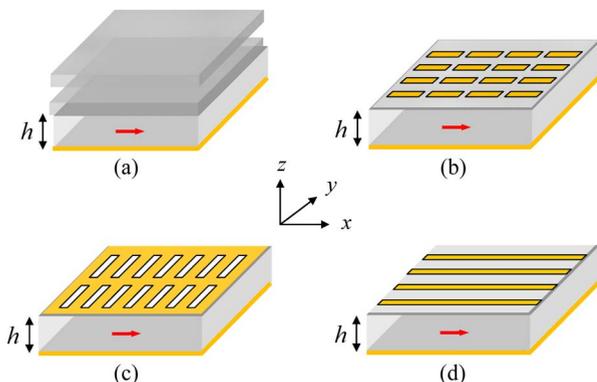

Fig. 6. *A side view of the multiple dielectric-superstrate PRS structure. A stack of high-permittivity dielectric layers separated by low permittivity spacer layers is used as the PRS. (Figure is adapted from [4].)*

(assuming low enough frequencies that printed-circuit fabrication is possible). In this case, the PRS is a 1-D periodic structure, with a period d between the wires or strips. In all cases, the thickness h of the substrate directly controls the beam angle θ_0 and determines whether the beam is a broadside beam ($\theta_0 = 0$) or a conical beam ($\theta_0 > 0$). The geometrical properties of the PRS control the beamwidth of the radiated beam (design formulas are given in Section II-F). In Fig. 5(a), the PRS is not planar (in the sense of being localized to a plane), though it will be relatively thin when using a single superstrate layer with a high permittivity. In Fig. 5(b)–(d), the PRS is completely planar or nearly so (assuming thin metallic conductors).

Fig. 6 shows a more detailed view of the dielectric-superstrate PRS structure of Fig. 5(a). For this structure a stack of high-permittivity layers, each with thickness t, is used. Fig. 6 assumes that the spacing layers between the high-permittivity superstrate layers have the same permittivity as the substrate layer, though this is not a necessary requirement. The optimum thickness of the high-permittivity superstrate layers is a quarter wavelength vertically, meaning that $k_{z2}t = \pi/4$, where k_{z2} is the vertical wavenumber inside the superstrate layer, corresponding to a beam angle θ_0 in free space by Snell's law. This vertical wavenumber is $k_{z2} = k_0\sqrt{n_2^2 - \sin^2\theta_0}$, where $n_2 = \sqrt{\varepsilon_{r2}\mu_{r2}}$ is the index of refraction of the superstrate layers. (More generally, a superstrate thickness corresponding to an odd number of quarter wavelengths could be chosen. Choosing a quarter wavelength gives the thinnest possible superstrate.) The optimum spacing s between the superstrate layers is one quarter of wavelength vertically in the low-permittivity spacing layer region, so that $k_{z1}s = \pi/4$ with $k_{z1} = k_0\sqrt{n_1^2 - \sin^2\theta_0}$ and $n_1 = \sqrt{\varepsilon_{r1}\mu_{r1}}$ [for this structure the notation ($\varepsilon_{r1}, \mu_{r1}$) is used instead of ($\varepsilon_r, \mu_r$) for the substrate]. More generally, an odd number of quarter wavelengths could be chosen for the spacing thickness, but this will result in a thicker structure. Assuming the same material for the substrate and the spacing layers as in Fig. 6, the optimum spacing layer thickness will be half of the substrate

Fig. 5. *Examples of PRS structures. (a) A multiple dielectric-superstrate PRS. (b) A periodic metal patch PRS. The length and width of the patches are L and W in the x- and y-directions. The periodic spacings are a and b in the x- and y-directions. (c) A periodic slot PRS. The lengths and widths of the slots are L and W in the y- and x-directions. The periodic spacings are a and b in the y- and x-directions. (d) A periodic wire or metal strip grating PRS. The width of the metal strips is W and the periodic spacing in the y-direction is d. (Figure is adapted from [62].)*
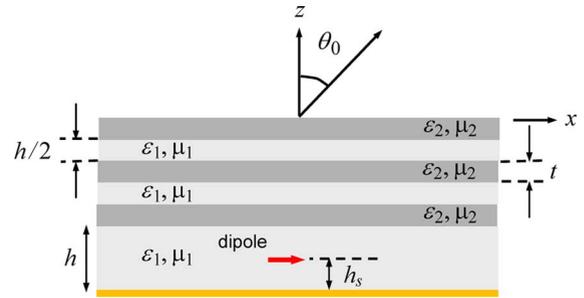
thickness, since the optimum substrate thickness is one half of a wavelength vertically in the substrate material, as explained in Section II-B.

B. Physics of Directive Beaming

The PRS structure of Fig. 1 acts like a leaky parallel-plate waveguide that is excited by a source. If the PRS were a perfectly conducting plate, the waveguide would be nonleaky and two types of parallel-plate waveguide modes TM_z and TE_z would be excited by an HED or HMD source. Each waveguide mode would have a vertical wavenumber k_{z1} given by $k_{z1}^{pp} = n\pi/h$. Assuming $\lambda_d/2 < h < \lambda_d$, where $\lambda_d = \lambda_0/n_1$ is the wavelength inside the substrate, only the lowest $n = 1$ pair of modes would be above cutoff. Both parallel-plate modes would have the same real-valued radial wavenumber k_ρ^{pp} and the fields would be described by magnetic and electric vector potentials of the form

$$A_z = A_{TM}^{pp} H_1^{(2)}\left(k_\rho^{pp}\rho\right)\cos\phi\cos(k_{z1}^{pp}z) \quad (TM_z) \qquad (1)$$

$$F_z = A_{TE}^{pp} H_1^{(2)}\left(k_\rho^{pp}\rho\right)\sin\phi\sin(k_{z1}^{pp}z) \quad (TE_z) \qquad (2)$$

where

$$k_\rho^{pp} = \sqrt{k_1^2 - \left(\frac{\pi}{h}\right)^2} \qquad (3)$$

and $k_1 = k_0 n_1$ is the wavenumber of the substrate, with $H_1^{(2)}$ the Hankel function corresponding to outward propagating waves (a time-harmonic convention of $\exp(j\omega t)$ is assumed and suppressed here). The field inside the parallel-plate region is a TM_x field for an x-directed HED excitation, and setting $H_x = 0$ gives the relation $A_{TE}^{pp}/A_{TM}^{pp} = -j\omega\varepsilon_1/k_{z1}^{pp}$. Similarly, a y-directed HMD would produce a TE_y field, so that $A_{TM}^{pp}/A_{TE}^{pp} = j\omega\mu_1/k_{z1}^{pp}$. The field inside the waveguide can thus be regarded as a sum of TM_z and TE_z modes or as a single mode that is purely TM_x or TE_y. The horizontal electric field of the parallel-plate modes is zero at the top and bottom conducting plates, and maximum halfway in between.

By replacing the top conducting plate of the parallel-plate waveguide with an isotropic homogeneous PRS such as a high-permittivity dielectric layer (or multiple layers), the modes remain TM_z and TE_z, but the power carried by each mode leaks through the top of the waveguiding structure (the PRS). Each parallel-plate mode then becomes a radiating leaky mode with a complex wavenumber $k_p = \beta - j\alpha$, where β is the phase constant and α is the attenuation (leakage) constant. The phase constant is still given *approximately* by (3), while the attenuation constant is determined by the geometrical properties of the PRS, discussed in Section II-F. The two modes now have differ-
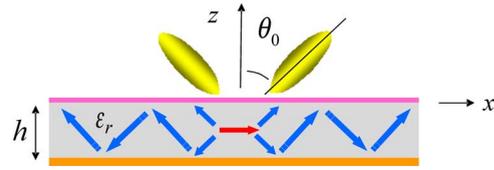

Fig. 7. *The PRS structure showing the leaky parallel-plate modes emanating from the dipole source. A conical beam radiated by the leaky modes is also shown.*

ent wavenumbers: $k_\rho^{TM} = \beta^{TM} - j\alpha^{TM}$ and $k_\rho^{TE} = \beta^{TE} - j\alpha^{TE}$. The phase constants of the leaky modes are approximately (though not exactly) equal, so that $\beta^{TM} \approx \beta^{TE} \approx k_\rho^{pp}$, and they correlate approximately with the radiated beam angle as

$$k_\rho^{pp} = k_0 \sin\theta_0. \qquad (4)$$

Fig. 7 pictorially illustrates the radially propagating leaky parallel-plate modes radiating to form a conical beam [as illustrated in Fig. 4(b)]. In the E-plane the beam is polarized with E_θ while in the H-plane it is polarized with E_ϕ.

By using (3) and (4), we obtain an approximate design equation for the substrate thickness in terms of the beam angle as

$$k_0 h = \frac{\pi}{\sqrt{n_1^2 - \sin^2\theta_0}}. \qquad (5)$$

For a broadside beam [Fig. 4(a)] where $\theta_0 = 0$, this reduces to $h = \lambda_d/2$. It is possible to design the PRS structure to use higher order parallel-plate modes instead of the $n = 1$ modes, in which case the numerator of (5) is replaced with $n\pi$. Since this leads to a thicker substrate, which is usually undesirable, only the $n = 1$ case is assumed henceforth.

For a broadside beam, the complex wavenumbers of the two leaky modes (TM_z and TE_z) are usually quite close, and become more so as the superstrate permittivity increases and the beam becomes narrower. The beam is thus a symmetric pencil beam with nearly equal beamwidths in the E- and H-planes. This interesting result actually holds true for all of the PRS structures shown in Fig. 5, regardless of the shape of the elements that make up the PRS. For example, the slots in Fig. 5(c) may be quite narrow, so that $W \ll L$, and the periods a and b may be quite different as well. Nevertheless, the broadside beam will be symmetric near the peak. For the conical beam, as the scan angle θ_0 increases, the beamwidths in the E- and H-planes begin to increasingly differ. In particular, the H-plane beamwidth becomes narrower as the scan angle θ_0 increases, while the E-plane beamwidth increases (this will be illustrated with

results in Section II-G). For the dielectric-superstrate PRS structure, this corresponds to the attenuation constants of the TE_z and TM_z modes differing by an increasing amount as the scan angle increases. Formulas for the beamwidth are given in Section II-F.

For a VED or VMD source inside the ideal parallel-plate structure, only a single parallel-plate mode is excited, either TM_z or TE_z, respectively. The corresponding vector potentials then have the respective forms

$$A_z = A_{TM}^{pp} H_0^{(2)} \left(k_\rho^{pp} \rho \right) \cos \left(k_{z1}^{pp} z \right) \qquad (6)$$

$$F_z = A_{TE}^{pp} H_0^{(2)} \left(k_\rho^{pp} \rho \right) \sin \left(k_{z1}^{pp} z \right). \qquad (7)$$

Because of the azimuthal symmetry of the corresponding leaky modes, the radiation patterns will always have a null at broadside. Hence, only a conical beam [Fig. 4(b)] can be created, polarized with E_θ for the TM_z case (VED) and E_ϕ for the TE_z case (VMD). The beams will be azimuthally symmetric for these sources.

For the ideal parallel-plate waveguide excited by an HED in the *x*-direction or an HMD in the *y*-direction, the field inside the waveguide will be either TM_x or TE_y. The two leaky modes TM_z and TE_z thus add together to give a single leaky mode that is polarized with a horizontal magnetic or electric field in the *y* or *x*-direction, respectively. This explains why the polarization of the radiated pattern is very nearly linearly polarized. For a dielectric-superstrate PRS the TM_z and TE_z leaky modes have different wavenumbers that depend on the scan angle, but the polarization of the pattern remains quite linear.

When the PRS is not an isotropic dielectric layer, but rather a metallic screen, the type of leaky mode that exists inside the structure depends on the type of PRS. For the metal patch structure of Fig. 5(b) with narrow patches ($W \ll L$), the field inside the substrate is essentially that of a single TM_x leaky mode if the substrate is air (otherwise it is a hybrid mode). For the slot type of PRS in Fig. 5(c) with narrow slots, the field is essentially a single TE_y leaky mode. For the wire or metal strip grating PRS in Fig. 5(d), the field is a single TM_x mode when the substrate is air. In all cases, the field on the radiating aperture is almost linearly polarized with an electric field in the *x*-direction. The wavenumber of the leaky mode will in general depend on the azimuth angle of propagation ϕ. This causes the conical beam to become increasingly asymmetric as the scan angle increases, just as for the dielectric layer PRS structure. One exception to this rule is the metal strip grating PRS structure in Fig. 5(d), for which the TM_x leaky mode has a wavenumber that is independent of azimuth angle. The reason for this interesting feature will be explained in Section II-G. This structure thus has a beamwidth that is independent of azimuth angle when radiating either a broadside beam or a conical beam.

C. Calculation of Radiation Patterns

The far-field radiation pattern $E_p(r, \theta, \phi)$ ($p = \theta, \phi$) of the PRS structure may be calculated in either of two ways: by Fourier transforming the aperture field at $z = 0$, or by using reciprocity. The reciprocity method is the computationally simplest approach. In this method, the far-field component $E_p(r, \theta, \phi)$ is calculated by placing an infinitesimal electric "testing" dipole in the far field, oriented in the *p*-direction, and then invoking the reciprocity theorem [20]. To illustrate, for the structure of Fig. 1 (HED source), the reaction $\langle a, b \rangle$ between the source dipole inside the substrate (the "a" source) and the testing dipole in the far field (the "b" source) oriented in the *p*-direction is

$$\langle a, b \rangle = \int_V \underline{E}^a \cdot \underline{J}^b \, dV = E_p(r, \theta, \phi). \qquad (8)$$

The reaction $\langle b, a \rangle$ between the testing dipole and the source dipole at $z = z_0$ is

$$\langle b, a \rangle = \int_V \underline{E}^b \cdot \underline{J}^a \, dV = E_x^b(0, 0, z_0). \qquad (9)$$

The field $E_x^b(0, 0, z_0)$ at the source dipole location due to the testing dipole in the *p*-direction in the far field can be determined by illuminating the structure with an incident plane wave polarized in the *p*-direction and with amplitude E_0 at the origin, where

$$E_0 = \left(\frac{-j\omega\mu_0}{4\pi r} \right) e^{-jk_0 r}. \qquad (10)$$

Hence, the incident plane wave is described by

$$\underline{E}^{inc} = \hat{p} E_0 e^{+j(k_x x + k_y y + k_z z)} \qquad (11)$$

where $k_x = k_0 \sin\theta \cos\phi$, $k_y = k_0 \sin\theta \sin\phi$, $k_z = k_0 \cos\theta$, for far-field observation angles (θ, ϕ). Equating the two reactions allows the far field to be determined. In mathematical form, the far-field components for the HED source at $z = z_0$ are given as

$$E_\theta(r, \theta, \phi) = \left(\frac{-j\omega\mu_0}{4\pi r} \right) e^{-jk_0 r} E_x^\theta(0, 0, z_0) \qquad (12)$$

$$E_\phi(r, \theta, \phi) = \left(\frac{-j\omega\mu_0}{4\pi r} \right) e^{-jk_0 r} E_x^\phi(0, 0, z_0) \qquad (13)$$

where $E_x^p(0, 0, z_0)$ $(p = \theta, \phi)$ denotes the E_x field at the source dipole location inside the substrate when the PRS structure is illuminated by an incident plane wave arriving from angles (θ, ϕ), polarized in the p-direction, and having a unit amplitude at the origin. When $p = \theta$ or ϕ the incident plane wave is a TM_z or TE_z plane wave, respectively.

A transmission-line model for the layered structure can be used to derive simple approximate formulas for the radiation pattern of the PRS structure. Inside the substrate and in the air region above the structure, the transverse (x and y components) of the plane-wave field can be modeled exactly as a voltage and current on corresponding transmission lines, where the characteristic impedance (or admittance) depends on the polarization. In particular

$$Z_i^{\text{TM}} = \frac{1}{Y_i^{\text{TM}}} = \frac{k_{zi}}{\omega \varepsilon_i} \quad (14)$$

and

$$Z_i^{\text{TE}} = \frac{1}{Y_i^{\text{TE}}} = \frac{\omega \mu_i}{k_{zi}} \quad (15)$$

where

$$k_{zi} = k_0 \sqrt{n_i^2 - \sin^2 \theta} \quad (16)$$

and $i = 0$ or 1, corresponding to the air or substrate regions, respectively. (For the air region this simplifies to $k_{zi} = k_0 \cos \theta$.) The transmission line model of the structure under plane-wave illumination is called the transverse equivalent network (TEN), and it is shown in Fig. 8. The voltage in the TEN models transverse electric field and the current models transverse magnetic field. The shunt susceptance B_L in Fig. 8 models the PRS, assuming a planar PRS as in Fig. 5(b)–(d). In particular, the shunt susceptance B_L in the TEN model is equal to the sheet susceptance of the planar PRS (with the sheet admittance of the

Fig. 8. *The TEN of the PRS structure. This is a transmission line model of the PRS structure that can be used to calculate the far-field pattern as well as the propagation wavenumber of the leaky modes.*

PRS defined as the ratio of the transverse electric field to the equivalent surface current flowing on the planar PRS for the fundamental Floquet wave). The shunt susceptance B_L can be either positive (capacitive PRS) or negative (inductive PRS). The PRS is capacitive in Fig. 5(b), and inductive in Fig. 5(c) and (d). After applying reciprocity, the far-field pattern is given by

$$E_\theta(r, \theta, \phi) = \left(\frac{-j\omega\mu_0}{4\pi r}\right) e^{-jk_0 r} \cos \phi \cos \theta \ V_1^{\text{TM}}(\theta, \phi) \quad (17)$$

$$E_\phi(r, \theta, \phi) = \left(\frac{j\omega\mu_0}{4\pi r}\right) e^{-jk_0 r} \sin \phi \ V_1^{\text{TE}}(\theta, \phi) \quad (18)$$

where $V_1^{\text{TM}}(\theta, \phi)$ is the voltage at the source dipole location $z = z_0$ in the TEN due to a unit-amplitude incident voltage wave impinging on the PRS from the air line (see Fig. 8) when TM_z admittances are used in the model. Similarly, $V_1^{\text{TE}}(\theta, \phi)$ corresponds to a unit-amplitude incident voltage wave and TE_z impedances in the model.

For the dielectric-superstrate PRS structure of Figs. 5(a) and 6 the PRS is not planar, and the model of Fig. 8 does not directly apply (although one can determine an equivalent shunt susceptance B_L and substrate thickness h that will allow the TEN model of Fig. 8 to correctly model the behavior of the nonplanar dielectric-superstrate PRS structure [21]). Instead, the TEN model of the dielectric-superstrate PRS structure consists of a cascade of transmission lines, which model the substrate, the superstrate layers, and the spacing layers in between [2], [4]. For the dielectric-superstrate PRS structure the functions V_1^{TM} and V_1^{TE} are independent of ϕ, since the characteristic admittances in the TEN are only functions of θ. For this structure, these voltage functions may be easily determined in closed form from simple transmission-line analysis [2], [4]. For other types of PRS structures, these voltage functions are usually dependent on both θ and ϕ since the shunt susceptance B_L in the TEN of Fig. 8 is generally dependent on both angles.

For the dielectric-superstrate PRS structure, the TEN model gives an exact calculation of the far field. For other types of PRS structures, where the PRS is composed of a planar periodic structure, the result from the TEN analysis is approximate, though usually very accurate. The approximation is due to the fact that the transmission line model in the TEN is based on the fundamental Floquet wave, and interactions between higher order Floquet waves and the ground plane are inherently neglected in the model. However, since the substrate is at least one-half of a wavelength thick in the dielectric [see (5)], these higher order interactions are usually small. For the periodic PRS structures the far-field pattern from the TEN analysis is known in closed form once the value of B_L is known. However, determining $B_L(\theta, \phi)$ requires the numerical solution of a periodic structure illuminated by a plane wave [9], [10].
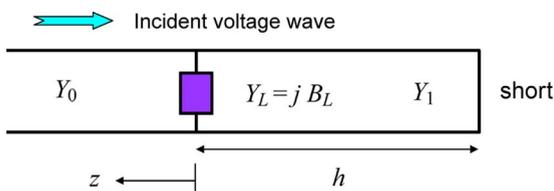
For an HED source located at a height of h_s above the ground plane as shown in Fig. 1, the far field from the TEN model is given by [13]

$$
\begin{aligned}
E_\theta(r, \theta, \phi) = &\left(\frac{-j\omega\mu_0}{4\pi r}\right) e^{-jk_0 r} \cos\phi \cos\theta \\
&\times \frac{2Y_0^{\mathrm{TM}}}{Y_0^{\mathrm{TM}} + j(B_L - Y_1^{\mathrm{TM}} \cot(k_{z1}h))} \\
&\times \left[\frac{\sin(k_{z1}h_s)}{\sin(k_{z1}h)}\right]
\end{aligned}
\tag{19}
$$

$$
\begin{aligned}
E_\phi(r, \theta, \phi) = &\left(\frac{j\omega\mu_0}{4\pi r}\right) e^{-jk_0 r} \sin\phi \\
&\times \frac{2Y_0^{\mathrm{TE}}}{Y_0^{\mathrm{TE}} + j(B_L - Y_1^{\mathrm{TE}} \cot(k_{z1}h))} \\
&\times \left[\frac{\sin(k_{z1}h_s)}{\sin(k_{z1}h)}\right].
\end{aligned}
\tag{20}
$$

The far-field pattern can also be determined by Fourier transforming the aperture field immediately above the PRS [22]. Fourier transforming the leaky-mode field allows one to calculate the far-field pattern of the leaky-mode(s) alone. This pattern can be compared with the total pattern in order to ascertain the dominance of the leaky mode(s). The calculation of the far-field pattern of a radially propagating leaky mode is fairly complicated and has been carried out only for the case of TM_z and TE_z leaky modes that propagate isotropically [5], meaning that the wavenumbers of each mode are independent of the azimuth angle ϕ. These are the types of modes that exist in the dielectric-superstrate PRS structure [20]. A simpler approach for calculating the *E*- and *H*-plane patterns of a general PRS structure is to assume a 1-D leaky-mode aperture distribution with a phase and attenuation constant chosen to match the values of the actual radial leaky mode for that plane. For example, to calculate the *H*-plane pattern ($\phi = \pi/2$) for a PRS structure excited by an *x*-directed HED or a *y*-directed HMD, a simple 1-D aperture distribution is assumed along the *y* axis, of the form

$$
E_x(y) = A e^{-jk_y^{LW}|y|}
\tag{21}
$$

where $k_y^{LW} = \beta - j\alpha$ is the complex wavenumber of the radial leaky mode at $\phi = \pi/2$. The far-field pattern in the *H*-plane is then given, to within a constant of proportionality, by [3]

$$
E_\phi(r, \theta, \pi/2) = \left(\frac{e^{-jk_0 r}}{r}\right) \cos\theta \int_{-\infty}^{\infty} E_x(y) e^{jk_0 y \sin\theta} \, dy
\tag{22}
$$

which yields

$$
E_\phi(r, \theta, \pi/2) = \left(\frac{e^{-jk_0 r}}{r}\right) \cos\theta \left[\frac{-j2k_y^{LW}A}{\left(k_y^{LW}\right)^2 - (k_0\sin\theta)^2}\right].
\tag{23}
$$

Similarly, for the *E*-plane pattern, an aperture distribution along the *x*-axis is assumed, of the form

$$
E_x(x) = A e^{-jk_x^{LW}|x|}.
\tag{24}
$$

The far-field pattern in the *E*-plane is then, to within a constant of proportionality

$$
E_\theta(r, \theta, 0) = \left(\frac{e^{-jk_0 r}}{r}\right) \int_{-\infty}^{\infty} E_x(x) e^{jk_0 x \sin\theta} \, dx.
\tag{25}
$$

(The $\cos\theta$ factor in (22) is absent in (25) because the equivalent magnetic current that models the aperture electric field is now flowing in a direction perpendicular to the observation plane rather than parallel to it.) This yields the result

$$
E_\theta(r, \theta, 0) = \left(\frac{e^{-jk_0 r}}{r}\right) \left[\frac{-j2k_x^{LW}A}{\left(k_x^{LW}\right)^2 - (k_0\sin\theta)^2}\right].
\tag{26}
$$

D. Substrate Design Formula

Equation (5) is an approximate result for the optimum substrate thickness, which assumes an ideal parallel-plate waveguide and hence ignores the loading effect of the PRS on the waveguide cavity. A more accurate expression may be developed by using (19) and (20) for the far-field pattern and then choosing the substrate thickness to maximize the power density radiated at the beam angle θ_0. This yields the result [13]

$$
h = h^{pp}\left(1 + \frac{\overline{Y}_1}{\pi \overline{B}_L}\right)
\tag{27}
$$

where h^{pp} is the substrate thickness predicted by the simple ideal parallel-plate waveguide analysis, given by (5). The term $\overline{Y}_1 = Y_1\eta_0$ is the characteristic admittance of the substrate transmission line in the TEN calculated at the beam angle θ_0, normalized by the intrinsic impedance of free space η_0. The normalized shunt susceptance $\overline{B}_L = B_L\eta_0$ is likewise calculated at angle θ_0. Using (14)

and (15), we have

$$\overline{Y}_1^{\text{TM}} = \frac{\varepsilon_{r1}}{\sqrt{n_1^2 - \sin^2 \theta_0}} \qquad (28)$$

$$\overline{Y}_1^{\text{TE}} = \frac{\sqrt{n_1^2 - \sin^2 \theta_0}}{\mu_{r1}}. \qquad (29)$$

The normalized characteristic admittance $\overline{Y}_1$ in (27) is either the TM or the TE value, depending on whether the beam is being optimized in the *E*-plane or the *H*-plane. Similarly, $\overline{B}_L$ is calculated assuming an incident plane wave polarized in the θ- or ϕ-directions incident at $\phi = 0$ or $\phi = 90°$, for the *E*- or the *H*-plane cases, respectively. Because the TM_z and TE_z admittances are different for $\theta_0 > 0$, the optimum substrate thickness will usually be slightly different for the two principal planes, so that the beam cannot be optimized simultaneously in both planes. (The metal-strip grating PRS of Fig. 5(d) is an exception, as explained later in Section II-G.) For a broadside beam, the optimum substrate thickness is unique since the TM_z and TE_z admittances are the same for $\theta_0 = 0$, and the susceptance value B_L is also unique. In this case, we have

$$\frac{h}{\lambda_0} = \left(\frac{1}{2n_1} \right) \left(1 + \frac{n_1}{\pi \overline{B}_L} \right). \qquad (30)$$

The $\overline{B}_L$ term in (30) accounts for the loading of the cavity by the reactive PRS.

Equations (27) and (30) assume a lossless planar PRS having a shunt susceptance B_L, so that the TEN model of Fig. 8 applies. For the dielectric-superstrate PRS structure of Fig. 6, the PRS consists of a stack of superstrate layers, which are of resonant (quarter-wavelength vertically) thickness and separation. Because of the resonant dimensions there is no detuning effect from the PRS, and maximum power density is radiated at θ_0 when (5) is satisfied. For a broadside beam, this means that $h = \lambda_d/2 = \lambda_0/(2n_1)$.

The TEN model of Fig. 8 can be used to calculate the wavenumbers of the leaky modes, in addition to the radiation pattern calculation that was discussed previously. The well-known transverse resonance technique is employed for this calculation [23], and the PRS is usually approximated as a constant isotropic sheet admittance for simplicity, so that B_L in the TEN model is independent of θ and ϕ [24]. When the optimum substrate thickness (30) is used to create a broadside beam, an analysis based on the TEN model of Fig. 8 shows that the TM_z and TE_z leaky modes have nearly the same wavenumber, and furthermore, the phase and attenuations constants are nearly the same [24], so that

$$\alpha^{\text{TM}} \approx \beta^{\text{TM}} \approx \alpha^{\text{TE}} \approx \beta^{\text{TE}}. \qquad (31)$$

For this optimum substrate condition, the power density radiated at broadside is maximum. This is not exactly the substrate thickness that optimizes the directivity of the beam (i.e., gives the narrowest beam). A further analysis reveals that the narrowest pencil beam at broadside occurs when the substrate thickness is slightly lower than the value from (30). In particular, the narrowest beam occurs when [24]

$$\beta/\alpha = \frac{\sqrt{3} - 1}{\sqrt{2}} \approx 0.518. \qquad (32)$$

The beam is then narrower than the beam corresponding to the "optimum" substrate thickness (which maximizes the power density at broadside) by a factor of $2^{1/4} \approx 1.19$ [24].

E. Design Restrictions

In addition to the design formulas (27) and (30) for the substrate thickness, there is also a design restriction that should be placed on the substrate in order to ensure only a single radiating beam for the case of a conical beam. For a conical beam, it is desired that only the $n = 1$ parallel-plate waveguide modes ($k_{z1}h = \pi$ for the ideal parallel-plate waveguide) be above cutoff, or else multiple conical beams will be created. To avoid having the $n = 2$ parallel-late waveguide modes propagate, the substrate thickness is limited to

$$\frac{h}{\lambda_0} < \frac{1}{\sqrt{\varepsilon_r \mu_r}}. \qquad (33)$$

Using (5), this leads to a maximum scan angle limit that depends on the substrate index of refraction, namely

$$\theta_0 < \sin^{-1} \left(\frac{\sqrt{3}}{2} n_1 \right). \qquad (34)$$

For an air substrate ($n_1 = 1$), the scan angle is limited to $60°$. In order to allow for a single conical beam that can scan down to endfire, the substrate must have a refractive index sufficiently large, satisfying

$$n_1 > \frac{2}{\sqrt{3}} \approx 1.15. \qquad (35)$$

For the case of a PRS constructed from a periodic structure [as in Fig. 5(b)–(d)], an additional restriction should be placed on the periodicity to avoid having higher

order Floquet waves propagate. Only the fundamental $(0,0)$ Floquet wave should propagate, as this wave is the one that corresponds to the parallel-plate waveguide mode that is modeled using the TEN of Fig. 8. Higher order Floquet waves that propagate will result in undesirable grating lobes in the radiation pattern. For periods a and b the necessary restriction is [9]

$$a < \lambda_0/2, \quad b < \lambda_0/2. \tag{36}$$

F. Radiation Characteristics

By starting with radiation formulas (19) and (20), it is possible to derive formulas for the important radiation characteristics of the antenna. This includes the peak field level radiated at the beam peak, the pattern beamwidth, and the pattern bandwidth [13]. All of these quantities depend on the value of B_L. From the beamwidth, an approximate expression for the directivity can be obtained in the case of a broadside pencil beam, since directivity for a pencil beam is approximately related to the E- and H-plane half-power beamwidths (angle in radians between the -3-dB points) as [22]

$$D = \frac{\pi^2}{\Delta\theta_E \, \Delta\theta_H}. \tag{37}$$

The pattern bandwidth is defined here as

$$BW = \frac{f_2 - f_1}{f_0} \tag{38}$$

where f_0 corresponds to the design frequency [for which the optimum substrate thickness is given by (27) or (30)], and the frequencies f_1 and f_2 are the lower and upper frequencies at which the power density radiated in the direction of angle θ_0 has dropped by a factor of one half (i.e., -3 dB) from the level at f_0. By combining formulas for the directivity and the bandwidth, we can also arrive at a formula for a figure of merit of the antenna, namely the directivity-bandwidth product.

Table 1 shows the peak field level radiated at the angle θ_0 in the E- and H-planes, assuming a unit-amplitude HED source located in the middle of the substrate, as shown in Fig. 1. For convenience, the spherical propagation term E_0 defined in (10) has been introduced to simplify the expressions. Results are shown for a broadside beam, a conical beam at a general scan angle θ_0, and an endfire beam $(\theta_0 \to \pi/2)$. (Recall that B_L is in general different for the E- and H-planes, and the appropriate value should be used. The value of B_L also depends on the scan angle, although the nature of the variation depends on the specific type of

Table 1 Expressions for Peak Field Value

	E-plane	H-plane
broadside	$\dfrac{2E_0\left\|\bar{B}_L\right\|}{n_1}$	$\dfrac{2E_0\left\|\bar{B}_L\right\|}{n_1}$
general scan angle	$\dfrac{2E_0\left\|\bar{B}_L\right\|}{n_1^2}\sqrt{n_1^2-\sin^2\theta_0}\cos\theta_0$	$\dfrac{2E_0\left\|\bar{B}_L\right\|}{\sqrt{n_1^2-\sin^2\theta_0}}$
endfire	$2E_0\dfrac{\sqrt{n_1^2-1}}{n_1^2}$	$\dfrac{2E_0\left\|\bar{B}_L\right\|}{\sqrt{n_1^2-1}}$

PRS.) It is seen that the peak field level increases as B_L increases. Table 1 also shows that, for a fixed value of B_L, as the beam angle θ_0 increases away from broadside, the radiated field level increases with scan angle in the H-plane but decreases in the E-plane. The table shows that for large B_L it is possible to obtain a high peak field level in the H-plane at endfire, but not in the E-plane.

Table 2 shows the -3-dB beamwidth in the E- and H-planes. It is seen that the beamwidth decreases as B_L increases. A larger value of B_L means that the PRS is acting more like a conducting plate, confining the fields to the substrate region and allowing for less leakage, lowering the attenuation constants of the leaky modes. As the attenuation constants of the leaky modes decrease, the effective size of the radiating aperture (where the fields of the leaky modes are significant) increases, narrowing the beam. Table 2 shows that the beamwidth of a broadside beam varies inversely with B_L, while the beamwidth of a conical beam varies inversely as B_L^2. Hence, it requires a more nearly ideal PRS (i.e., one closer to a perfectly conducting plate) to obtain narrow beams in the broadside case than in the scanned case. Table 2 also shows that, for a fixed value of B_L, as the scan angle increases the H-plane pattern becomes narrower while the E-plane pattern becomes broader. For a fixed value of B_L, a narrow conical beam can

Table 2 Expressions for Beamwidth

	E-plane	H-plane
broadside	$2\sqrt{\dfrac{2n_1^3}{\pi \bar{B}_L^2}}$	$2\sqrt{\dfrac{2n_1^3}{\pi \bar{B}_L^2}}$
general scan angle	$\dfrac{2n_1^2\sqrt{n_1^2-\sin^2\theta_0}}{\pi \bar{B}_L^2 \sin\theta_0 \cos^2\theta_0}$	$\dfrac{2\left(\sqrt{n_1^2-\sin^2\theta_0}\right)^3}{\pi \bar{B}_L^2 \sin\theta_0}$
endfire	*narrow beam not possible*	$\dfrac{2\left(\sqrt{n_1^2-1}\right)^3}{\pi \bar{B}_L^2}$

Table 3 Expressions for Pattern Bandwidth

	E-plane	**H-plane**
broadside	$\dfrac{2n_1}{\pi \overline{B}_L^2}$	$\dfrac{2n_1}{\pi \overline{B}_L^2}$
general scan angle	$\dfrac{2n_1^2 \sec \theta_0}{\pi \overline{B}_L^2 \sqrt{n_1^2 - \sin^2 \theta_0}}$	$\dfrac{2\sqrt{n_1^2 - \sin^2 \theta_0}}{\pi \overline{B}_L^2 \sec \theta_0}$
endfire	*narrow beam not possible*	0

be obtained down to the endfire limit in the *H*-plane, but not in the *E*-plane.

Table 3 shows the pattern bandwidth. The bandwidth is inversely proportional to B_L^2 for both broadside and conical beams. Hence, as the beam gets narrower, the bandwidth decreases. Table 3 also shows that the bandwidth decreases with θ_0 in the *H*-plane and increases in the *E*-plane, which is the same trend as for the beamwidth.

The product of directivity and pattern bandwidth for a broadside beam can be calculated by using (37) along with Tables 2 and 3. The result for this figure of merit is

$$D \cdot BW = \frac{2.47}{n_1^2}. \tag{39}$$

(In [36] the factor 2.47 was erroneously reported as 4.0.) The figure of merit for the PRS antenna is thus largest when the substrate is air ($n_1 = 1$).

The reciprocity method can only be used to easily determine the far-field pattern when the structure is infinite in the horizontal directions. On the other hand, the leaky-wave method can be easily extended to calculate the pattern of a structure with a finite aperture that is terminated with an ideal absorber at the boundary. In this case, the far field of the aperture within the finite aperture is Fourier transformed to obtain the pattern [25]. Near the peak of the beam, the shape of the pattern in the *E*- and *H*-planes is usually well predicted by using a simple 1-D leaky-wave radiation formula, as shown by (26) and (23), respectively.

Equations (26) and (23) can be used to determine the *E*- and *H*-plane beamwidths in terms of the attenuation constants α^{TM} and α^{TE} of the leaky modes propagating in the directions $\phi = 0$ and $\phi = 90°$, respectively. This leads to the following beamwidth results for a conical beam at an angle $\theta_0 > 0$:

$$\Delta \theta_E = \frac{2\alpha^{\mathrm{TM}}}{\cos \theta_0} \tag{40}$$

and

$$\Delta \theta_H = \frac{2\alpha^{\mathrm{TE}}}{\cos \theta_0}. \tag{41}$$

For a broadside beam that arises from a pair of leaky modes with $\alpha^{\mathrm{TM}} \approx \beta^{\mathrm{TM}} \approx \alpha^{\mathrm{TE}} \approx \beta^{\mathrm{TE}}$ [see (31)], corresponding to an optimum beam with maximum power density radiated at broadside, the symmetrical beam has equal *E*- and *H*-plane beamwidths given by

$$\Delta \theta_E = \Delta \theta_H = 2\sqrt{2}\alpha \tag{42}$$

where α denotes the (unique) value of the attenuation constant. Note the extra factor of $\sqrt{2}$ in the broadside formula compared to the conical beam case. (The broadside formula is not a smooth continuation of the conical formula as the beam angle θ_0 approaches zero.) For beam angles θ_0 that are sufficiently close to broadside, but not exactly at broadside, neither formula will be accurate, and the beam will be somewhat between a pencil beam and a conical beam in shape.

Using (40)–(42) together with Table 2, which expresses the beamwidths in terms of the normalized PRS susceptance $\overline{B}_L = \eta_0 B_L$ (where B_L is in general different in the *E*- and *H*-planes), it is then possible to express the attenuations constants in terms of $\overline{B}_L$. Results are omitted for brevity.

G. Results

A typical far-field radiation pattern for the slot PRS structure of Fig. 5(c) is shown in Fig. 9 at 12 GHz for a nonmagnetic substrate with $\varepsilon_r = 2.2$. Fig. 9(a) and (b) shows the *E*- and *H*-plane patterns for a broadside beam, respectively, where the substrate thickness is $h = 1.33$ cm. The exact pattern is shown, calculated by using reciprocity along with a periodic method-of-moments (MoM) code in order to compute the functions $E_x^p(0, 0, z_0)$ in (12) and (13). Also shown is the pattern calculated using the TEN, using (19) and (20). For the TEN calculation a periodic MoM code was used to determine the value of B_L in the *E*- and *H*-planes for each angle θ of plane-wave incidence [9], [10]. The results show that the TEN model is very accurate. Fig. 9(c) and (d) shows similar results for a conical beam at a scan angle of $\theta_0 = 45°$, for which the substrate thickness is $h = 1.90$ cm. Note that the *E*- and *H*-plane beamwidths are nearly identical for the broadside beam, but for the conical beam the *H*-plane pattern has a narrower beam. This difference in beamwidths increases as the scan angle θ_0 increases, as expected from Table 2. Fig. 10 shows the normalized susceptance $\overline{B}_L$ as a function
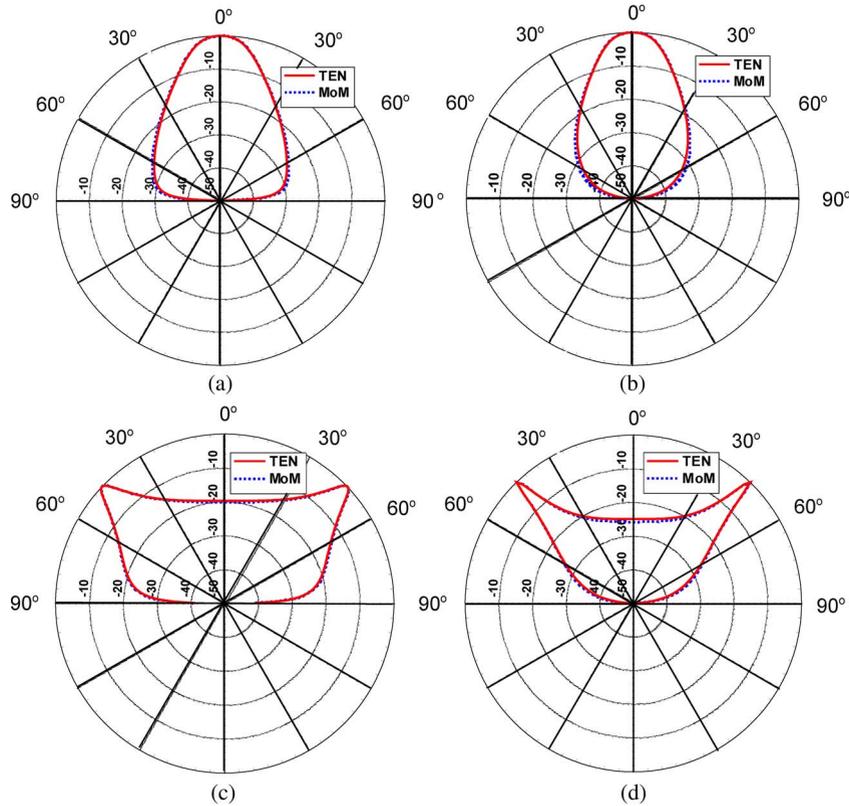
Fig. 9. *Far-field radiation patterns for the slot PRS structure of Fig. 5(c) at 12 GHz, using a substrate with $\varepsilon_r = 2.2$. (a) E-plane pattern for a broadside design. (b) H-plane pattern for a broadside design. (c) E-plane pattern for a 45° scan angle. (d) H-plane pattern for a 45° scan angle. For the broadside case the substrate thickness is h = 1.33 cm. For the conical beam the substrate thickness is h = 1.90 cm. The other dimensions are L = 0.6 cm, W = 0.05 cm, a = 1.0 cm, b = 0.3 cm. (Figure is from [10].)*

of angle θ in the *E*- and *H*-planes for this slot PRS [26]. It is seen that there is some variation with angle, though the variation is not large.

Fig. 11 shows a practical realization of the dielectric-superstrate PRS structure of Fig. 6, using a single high-

Fig. 10. *Normalized susceptance of the slot PRS used in Fig. 9 as a function of incidence angle θ for the E-plane (TM$_z$ incidence, $\phi = 0$) and the H-plane (TE$_z$ incident, $\phi = 90°$).*

permittivity superstrate layer. The structure is designed for a millimeter-wave frequency of 62.2 GHz, and uses a superstrate with a relative permittivity of $\varepsilon_{r2} = 55$ and an air $(\varepsilon_{r1} = 1)$ substrate. The high-permittivity ceramic superstrate has a thickness of 0.484 mm, which is three times the usual value of $t = \lambda_{d2}/4 = 0.16$ mm, in order to keep the superstrate from getting too thin. The structure is fed by a slot in the ground plane that is excited by a wave-guide. Absorber is placed around the perimeter to reduce reflections of the leaky modes at the boundary. The calculated pattern of the finite-radius structure is obtained by calculating the aperture field for an infinite structure and then Fourier transforming that part of the aperture field that is within the circular aperture [25]. A measured pattern is also compared, and the agreement is good for both the *E*- and *H*-planes.

Fig. 12 shows the *H*-plane pattern of a dielectric-superstrate PRS structure with a single superstrate of $\varepsilon_{r2} = 10$ over a substrate with $\varepsilon_{r1} = 2.1$, comparing the total pattern (from reciprocity) with the leaky-wave pattern obtained from (23) [3]. The agreement is excellent, supporting the fact that the leaky mode is the dominant contributor to the aperture field of the antenna.
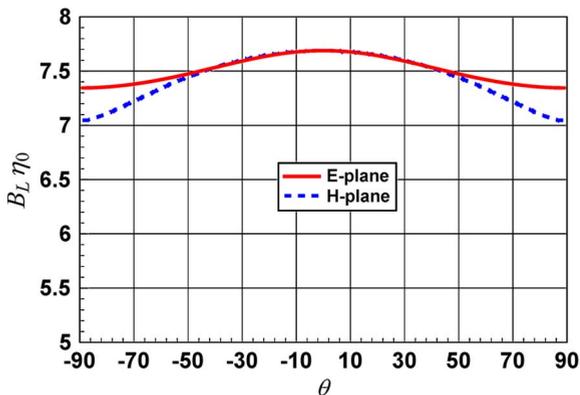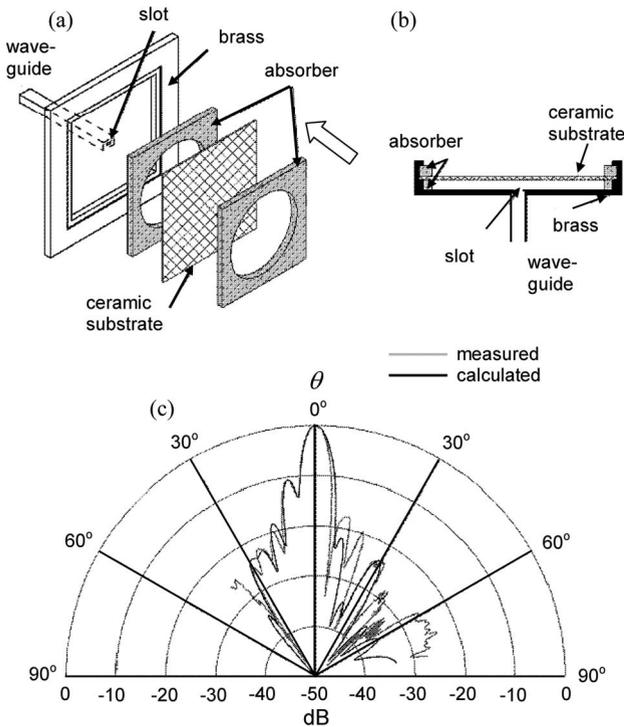
Fig. 11. *A dielectric-superstrate PRS structure designed for a millimeter-wave frequency of 62.2 GHz. A single high-permittivity superstrate layer is used as the PRS. (a) Three-dimensional view of the structure. (b) Side view of the structure. (c) Radiation patterns (E-plane pattern on the left side, H-plane pattern on the right side). An air substrate with thickness h = 2.41 mm is used along with a ceramic superstrate having ε_{r2} = 55 and a thickness t = 0.484 mm. The radius of the aperture is 3.73 λ_0. (Figure is from [25].)*

metal patches) can propagate on the rather thick substrate layer. Although the surface wave itself does not radiate (being a slow wave) radiation from a higher order Floquet wave of the perturbed surface wave (which is now a leaky wave due to the perturbations) occurs, and this evidently produces the secondary beams.

The slot PRS structure does not suffer from the surface-wave problem, since the structure only supports parallel-plate waveguide modes, which (perturbed by the slots) become the leaky modes. Fig. 15 shows the radiation pattern for the slot PRS structure at 12 GHz, using a substrate with $\varepsilon_r = 2.2$ and varying substrate thicknesses. (The patterns are normalized so that the H-plane pattern has a peak at 0 dB, for convenience, so the E- and H-plane patterns can be easily compared.) The beam is shown scanning to 75° (though even larger scan angles are possible) without any secondary beam problem. However, as noted above in connection with Table 2, the beam-widths and peak power levels increasingly differ between the E- and H-plane patterns as the beam scans toward endfire.

The wire or metal-strip grating PRS in Fig. 5(d) enjoys a unique property that the others do not, namely that the leaky-mode propagation on the structure is omnidirectional, provided the substrate is air [27]. In particular, the structure of Fig. 5(d) then supports a pure TM_x leaky mode, whose electric field is polarized parallel to the metal wires or strips. Because of the interesting spatial dispersion property of the metal strip grating, this leaky mode has a complex wave number k_ρ that is independent of the
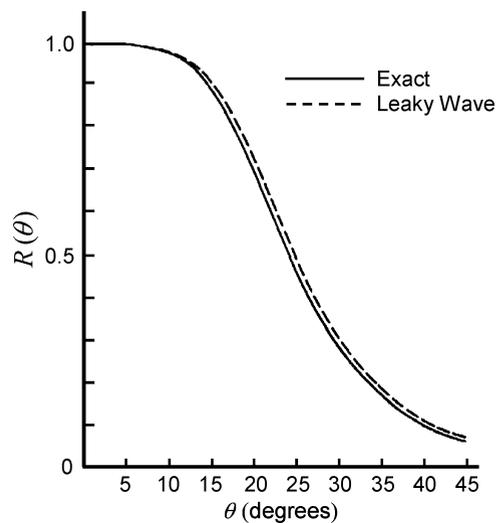
Fig. 13 shows patterns for a metal patch PRS structure [Fig. 5(b)] for varying substrate thicknesses, using an air substrate at a frequency of 12 GHz. In Fig. 13(a), the substrate thickness is varied so that the beam scans from broadside to 45°. In Fig. 13(b), the substrate thickness is increased further so that the beam scans to 60° and 75°. As expected from (34), for a scan angle beyond 60° an undesirable secondary beam forms. This is especially pronounced for the 75° scan, where a secondary beam (pointing at about 43°) is larger than the primary beam at 75°. Another secondary beam at about 12° is also observed in this case.

As design formula (35) suggests, one way to avoid the secondary beam problem is to increase the substrate permittivity. However, the use of a substrate with $\varepsilon_r > 1$ leads to undesirable E-plane patterns for the metal patch PRS structure. Fig. 14 shows the E-plane pattern that results when using a substrate with $\varepsilon_r = 2.2$, designed for a broadside beam at 12 GHz ($h = 0.843$ cm). As seen, the pattern is very corrupt, with large secondary beams pointing at about 20°, which overshadow the main beam at broadside. These secondary beams are due to the fact that a surface wave (perturbed somewhat by the presence of the

Fig. 12. *A comparison of the exact and leaky-wave normalized H-plane power density patterns (denoted as R(θ)) for a dielectric-superstrate PRS structure using a single high-permittivity superstrate layer as the PRS. The substrate has $\varepsilon_{r1} = 2.1$ and has a thickness of $\lambda_{d1}/2$. The superstrate has $\varepsilon_{r1} = 10.0$ and a thickness of $\lambda_{d2}/4$. The structure is excited by a horizontal electric dipole in the middle of the substrate. (Figure is from [3].)*
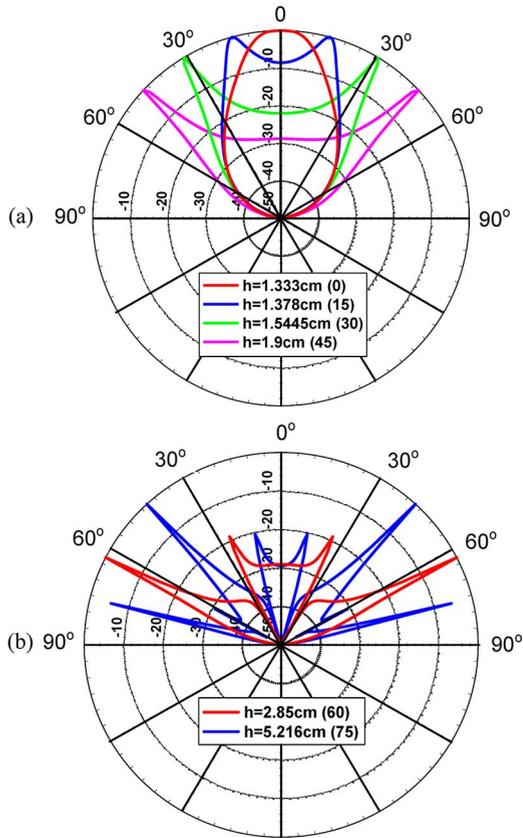
Fig. 13. *H-plane radiation patterns for the patch PRS structure of Fig. 5(b) at a frequency of 12 GHz for an air substrate. Various substrate thicknesses h are used to obtain different scan angles. (a) The substrate thicknesses are: 1.333 cm (0° scan), 1.378 cm (15° scan), 1.545 cm (30° scan), 1.900 cm (45° scan). (b) The substrate thicknesses are: 2.850 cm (60° scan), 5.216 cm (75° scan). The other dimensions are L = 1.25 cm, W = 0.1 cm, a = 1.35 cm, b = 0.3 cm. (Figure is from [9].)*

the type of PRS (see Fig. 10 for a typical example involving the slot PRS). In any case, the general result that the beamwidth variation with ϕ increases as the scan angle θ_0 increases is usually true for most PRS structures, as evidenced by the results of Fig. 15 for the slot PRS structure.

For the metal-strip grating PRS, however, the situation is somewhat unique. The shunt susceptance B_L still varies as a function of ϕ, but it does so in a way that precisely compensates for the natural change in the characteristic admittance of the substrate transmission line in the TEN model as we change from the E-plane to the H-plane. Notice that the ratio of characteristic admittances for the E- and H-planes is, from (28) and (29)

$$\frac{Y_1^{TE}}{Y_1^{TM}} = \frac{Z_1^{TM}}{Z_1^{TE}} = 1 - \frac{\sin^2 \theta_0}{n_1}. \qquad (43)$$

When the substrate is air ($n_1 = 1$), this becomes $Y_1^{TE}/Y_1^{TM} = \cos^2 \theta_0$. For a fixed B_L, this difference in the characteristic admittances would mean that we have very different beam properties in the E- and H-planes as θ_0 increases and the ratio of admittances becomes significantly different than unity. This explains the trends seen in Table 2. However, for the metal-strip grating illuminated by a TM_x plane wave, the sheet susceptance of the grating, and hence the shunt susceptance B_L in the TEN, is inversely proportional to the term $k_0^2 - k_x^2$, where k_x is the wave number of the plane wave in the x-direction (parallel to the strip axis) [27]. The ratio of this susceptance between the E- and H-planes is thus $B_L^{TM}/B_L^{TE} = 1/\cos^2 \theta_0$, which exactly matches the ratio of the characteristic

azimuth angle of propagation ϕ. This in turn results in a radiation pattern that has a beam pointing angle θ_0 and a beamwidth $\Delta\theta$ that are both independent of ϕ [27]. For the other types of PRS structures shown in Fig. 5, the beam angle θ_0 is approximately constant as ϕ changes [as predicted by (5)], but not exactly so. This is a consequence of the fact that the optimum substrate thickness for producing a beam at angle θ_0 is not constant, but depends on ϕ. This is seen from (27), (28), and (29), which shows that the optimum substrate thickness is different in the E- and H-planes. Also, for the PRS structures in Fig. 5(a)–(c) the beamwidth is not independent of ϕ, with the amount of variation increasing as the scan angle θ_0 increases. This is consistent with Table 2, which shows that for a fixed value of $\overline{B}_L = B_L\eta_0$, the beamwidth in the H-plane decreases while the beamwidth in the E-plane increases as the scan angle θ_0 increases. For any specific PRS, the value of B_L will usually not be constant but will change as a function of the scan angle θ_0, though the variation with θ_0 may be mild, depending on
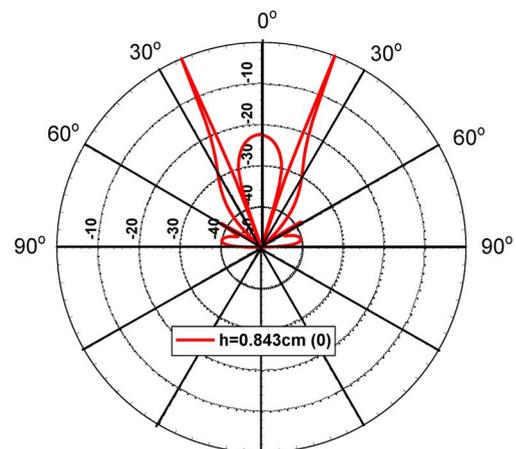

Fig. 14. *E-plane radiation pattern for the patch PRS structure of Fig. 5(b) at a frequency of 12 GHz, for a substrate with $\varepsilon_{r1} = 2.2$. The substrate thickness is h = 0.843 cm, corresponding to a broadside beam. The other dimensions are L = 1.25 cm, W = 0.1 cm, a = 1.35 cm, b = 0.3 cm. (Figure is from [9].)*

admittances. Hence, the reflection of TM_x planes waves from the PRS is the same in the *E*- and the *H*-planes, and this results in the wavenumber of the TM_x leaky mode being the same in both planes. In fact, the wavenumber of the TM_x leaky mode turns out to be completely independent of ϕ, since the characteristic admittance of the TM_x plane wave is inversely proportional to $k_0^2 - k_x^2$, a result that holds for all angles of incidence (θ, ϕ) [27].

To confirm this remarkable omnidirectional property, Fig. 16 shows *E*- and *H*-plane patterns for a metal-strip grating structure when an *x*-directed HED source in the middle of an air substrate is used. It is seen that the *E*- and *H*-plane patterns are nearly identical, even for large scan angles. Although the TM_x leaky mode has the same wavenumber in both the *E*- and the *H*-planes, the two patterns are not exactly the same in Fig. 16, since the radiated power density is different in the two planes
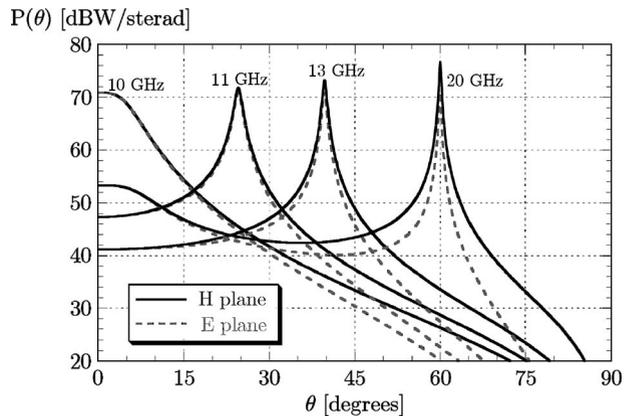

Fig. 16. *A comparison of* E- *and* H-*plane patterns for the metal-strip grating PRS structure of Fig. 5(d) using an air substrate, for four different frequencies (10, 11, 13, 20 GHz). The frequencies correspond to broadside (10 GHz) and three different scan angles. The substrate thickness is* h = 1.437 cm. *The width of the metal strips is* w = 0.52 mm *and the period is* d = 3 mm. *(Figure is from [27].)*
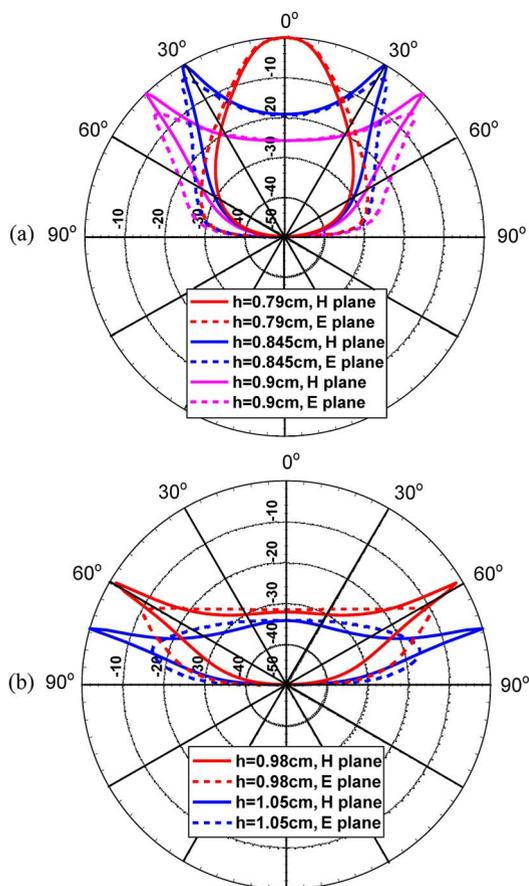
(though not as different as for other types of PRS structures). Hence, for larger scan angles some difference in the patterns is evident. Fig. 17 further shows the complete polar pattern for two cases, broadside [Fig. 17(a)] and a $40°$ scan angle [Fig. 17(b)]. These results show quite good omnidirectionality for both the broadside case and the conical beam case. The omnidirectionality for the broadside case is not surprising, since it was noted earlier that a nearly symmetric pencil beam at broadside is produced by any PRS structure operating at broadside. However, the omnidirectional nature of the conical beam is remarkable, especially considering that the metal-strip grating itself is very unidirectional in physical appearance.

III. METAMATERIAL SLAB LEAKY-WAVE ANTENNA

A. Introduction

The metamaterial slab leaky-wave antenna consists of a grounded artificial slab of thickness *h* having a positive but very low relative permittivity $\varepsilon_r \ll 1$ excited by a source inside the slab. The structure is shown in Fig. 2, where the artificial low-permittivity substrate is realized by using a wire medium with a closely spaced periodic arrangement of metallic wires. The perfectly conducting wires have a radius *a* and a periodic spacing of *d*. Fig. 2 shows a line source that is invariant in the *y*-direction. A line source is used here for simplicity (with consequently no variation of the fields in the *y*-direction), though a dipole source could also be used. Assuming that *d* is small relative to a wavelength, the wire medium acts as a homogeneous artificial medium with a relative permittivity that is described by the lossless Drude equation [28]–[31]. For the case of a
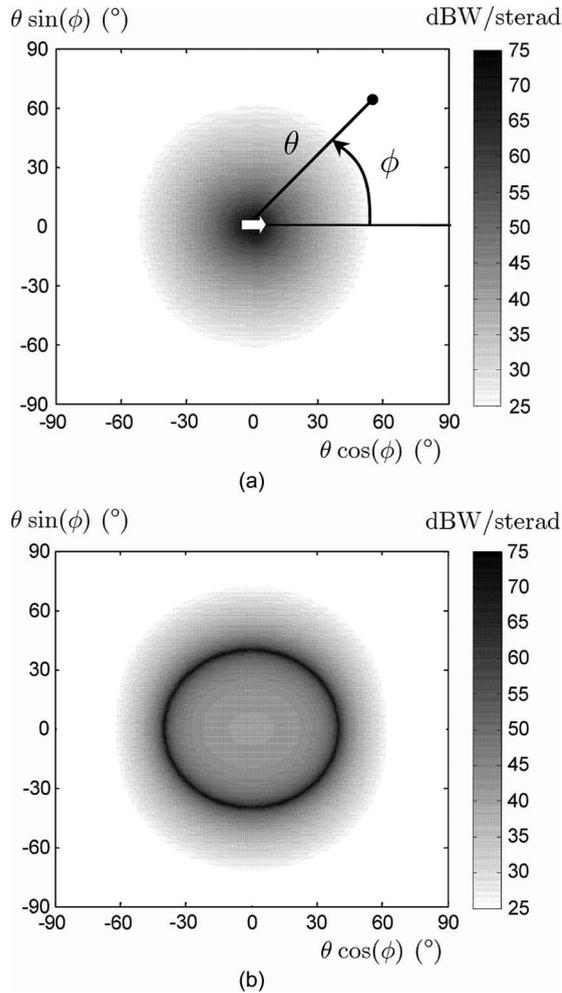

Fig. 15. E- *and* H-*plane patterns for the slot PRS structure of Fig. 5(c) at a frequency of 12 GHz, for a substrate with* ε_{r1} = 2.2. *Various substrate thicknesses* h *are used to obtain different scan angles. The* H-*plane patterns are shown with a solid line while the* E-*plane patterns are shown with a dashed line. (a) The substrate thicknesses are: 0.790 cm ($0°$ scan), 0.845 cm ($30°$ scan), 0.900 cm ($45°$ scan). (b) The substrate thicknesses are: 0.980 cm ($60°$ scan), 1.050 cm ($75°$ scan). The other dimensions are* L = 0.6 cm, W = 0.05 cm, a = 1.0 cm, b = 0.3 cm. *(Figure is adapted from [10].)*

Fig. 17. *A polar representation of the far-field pattern for the metal-strip grating PRS structure of Fig. 16. (a) A broadside beam at 10 GHz. (b) A conical beam with a scan angle of 40° at 13 GHz. (Figure is from [27].)*

line-source excitation where there is no *y* variation ($k_y = 0$), the Drude equation is

$$\varepsilon_r = 1 - \left(\frac{f_p}{f}\right)^2 \qquad (44)$$

where f_p is called the plasma frequency since the medium simulates an artificial plasma. Assuming that $a \ll d$, the plasma frequency is given approximately as [32]

$$f_p = \frac{c}{d} \frac{1}{\sqrt{2\pi\left(\ln\dfrac{d}{2\pi a} + 0.5275\right)}} \qquad (45)$$

where *c* is the speed of light in air. Note that a small but positive relative permittivity results when the frequency of operation is above, but close to, the plasma frequency.

B. Physics of Directive Beaming

Fig. 18 shows a side view of the structure, along with a ray picture that helps to explain some of the physics. According to Snell's law, rays emanating from the line source will be bent towards the normal, as shown in Fig. 18, when the effective relative permittivity of the slab is small and positive. One would then naturally expect a radiated beam that would be focused towards broadside, and indeed this happens regardless of the thickness *h* of the substrate. For a *semi-infinite* slab of artificial material with an interior source located at some distance from the interface, the ray picture offers a complete explanation of the narrow beam phenomenon. However, for a *finite-thickness slab* of artificial material, as shown in Fig. 18, it has been observed that a significant further narrowing of the beam beyond that expected from Snell's law can be obtained by properly optimizing the thickness of the artificial substrate [33]. It has been found that the optimum substrate thickness corresponds to [34], [35]

$$k_0 h \sqrt{\varepsilon_r} = n\pi \qquad (46)$$

where $n = 1$ gives the thinnest possible slab. This equation is exactly the same condition for the optimum substrate thickness for the PRS structures, for a broadside beam, if the detuning effect of the PRS is ignored. That is, (46) is the same as (30) when using $n = 1$, if the B_L term in (30) is ignored. For a given value of the slab thickness *h*, (46) and (44) can be combined into an equation for the optimum frequency, which is

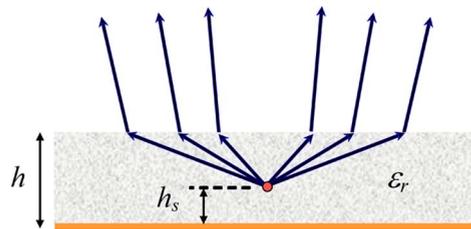$$f_{opt} = \sqrt{f_p^2 + \frac{n^2 c^2}{4h^2}}. \qquad (47)$$

Fig. 18. *A low-permittivity metamaterial slab on a ground plane with a line source inside of the slab. An illustration of rays emanating from the source and bending towards the normal in the air region is also shown. (Figure is adapted from [34].)*

The significant narrowing of the beam when the optimum slab thickness is used has been found to be attributable to the excitation of a weakly attenuated leaky mode that can propagate on the grounded artificial slab [33]–[35]. Analysis has shown that when the optimum substrate thickness from (46) is used, the leaky mode (which is a TE$_z$ mode, where z is the normal direction) has phase and attenuation constants given by [34]

$$\beta^{\mathrm{TE}} \approx \alpha^{\mathrm{TE}} \approx k_0 \sqrt{\frac{\varepsilon_r^{3/2}}{n\pi}}. \qquad (48)$$

As the effective relative permittivity decreases (by operating closer to the plasma frequency), the attenuation constant also decreases, resulting in a narrower beam. Note that for the optimum slab thickness the phase and attenuation constants of the leaky mode are nearly equal, a condition that was also observed in Section I for a broadside beam with the PRS structures.

C. Results

Fig. 19 shows a comparison of the far-field pattern in the *H*-plane (*xz*-plane) for a grounded wire-medium slab consisting of six layers of circular wires over a ground plane that is excited by a line source. For the parameters used here ($a = 0.5$ mm, $d = 20$ mm), (45) yields a plasma

Fig. 20. *(a) Aperture field distribution and (b) H-plane far-field pattern for an electric line source inside of a homogenized low-permittivity slab on a ground plane. Results are shown at 20.5, 20.039, and 20.155 GHz. The slab has a thickness of h = 60 mm and a plasma resonance frequency of f_p = 20 GHz. The line source is located in the middle of the slab. In (a) the total field (TF), leaky-wave field (LWF) and space-wave field (SPWF) are shown. In (b) the pattern from the total aperture field (TF) is shown along with the pattern from the leaky-wave field (LWF) on the aperture. (Figure is from [34].)*
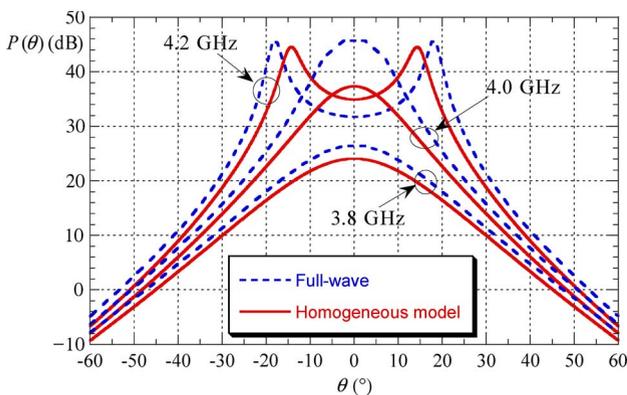
Fig. 19. *H-plane radiation patterns for the structure of Fig. 18, where the metamaterial slab is composed of a wire medium as shown in Fig. 2. The numerically exact pattern of the line source inside of the wire medium structure is compared with the pattern of the line source inside of a homogenized low-permittivity slab. The radius of the wires is a = 0.5 mm and the periodic spacing in the x- and z-directions is d = 20 mm. This corresponds to a plasma resonance frequency of 3.877 GHz. There are six rows of wires in the artificial slab, with the first row centered at a height of d/2 above the ground plane. The electric line source is located in the middle of the slab. The optimum frequency for broadside radiation is 4.07 GHz. (Figure is from [34].)*
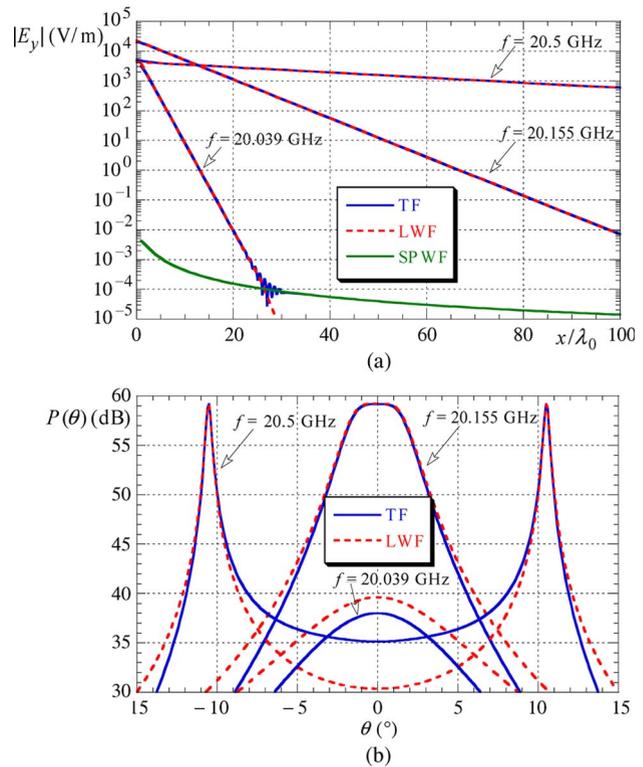
frequency f_p of 3.877 GHz. The optimum frequency for broadside radiation from (47) is 4.07 GHz, for which $\varepsilon_r = 0.093$ from (44). The far-field pattern is calculated in two different ways. The first method uses an homogenized slab model [i.e., a line source inside of a homogeneous grounded slab, with a small relative permittivity that is given by (44) and (45)]. The second method uses the actual wire-medium structure. In the latter case, a numerical periodic MoM solution was used along with reciprocity to calculate the far-field pattern [34]. The agreement is fairly good, except for a slight shift in the frequency, which may be due in part to the difficulty in deciding the best equivalent thickness to use for modeling the homogenized wire-medium slab. For this calculation, an extension of $d/2$ above the centers of the top row of wires was used to define the interface of the homogenized slab.

Fig. 20(a) shows a comparison of the exact aperture field on top of an artificial slab when excited by a line source, and the field of the leaky mode. The calculation assumes a homogenized dielectric slab with a small

Table 4 Comparison of PRS and Metamaterial LWAs

PRS	Metamaterial	Metamaterial Non-dispersive
$D = \dfrac{1.24}{(\alpha/k_0)^2}$	$D = \dfrac{1.24}{(\alpha/k_0)^2}$	$D = \dfrac{1.24}{(\alpha/k_0)^2}$
$BW = \dfrac{2}{\varepsilon_r}(\alpha/k_0)^2$	$BW = 2(\alpha/k_0)^2$	$BW = \dfrac{2}{\pi^{2/3}}(\alpha/k_0)^{2/3}$
$D \cdot BW = \dfrac{2.48}{\varepsilon_r}$	$D \cdot BW = 2.48$	$D \cdot BW = \dfrac{2.48}{\pi^{2/3}}\dfrac{1}{(\alpha/k_0)^{4/3}}$

relative permittivity, as given by (44) and (45). For this structure, the effective slab permittivity is $\varepsilon_r = 0.0153$ at 20.155 GHz, which is the optimum broadside frequency from (47). The total field consists of the leaky-wave field and a space-wave field, which is the leftover part of the total field that is not part of the leaky-wave field. The agreement between the total field and the leaky-wave field is excellent, verifying that this structure is indeed operating as a leaky-wave antenna. Further confirmation is provided in Fig. 20(b), which shows the far-field *H*-plane pattern for the same structure in Fig. 20(a). The agreement between the total pattern and the pattern of the leaky mode is excellent.

An analysis of the directivity and pattern bandwidth for an HED source inside of a metamaterial slab has been carried out [36]. The results are summarized in Table 4. Table 4 shows a comparison of results for three structures: 1) a PRS leaky-wave antenna, as discussed in Section II; 2) a metamaterial slab structure as discussed here, where the relative permittivity obeys the lossless Drude equation (44); and 3) the same metamaterial slab structure that has a hypothetical constant relative permittivity that does not change with frequency (i.e., a dispersionless slab material), which is equal to that of the actual wire-medium slab at the design frequency. Also included in Table 4 is the figure of merit defined as the product of the directivity and the pattern bandwidth. It is seen that the figure of merit for the metamaterial antenna is the same as that of the PRS antenna when an air substrate is used for the PRS antenna. Interestingly, the figure of merit is significantly higher for the hypothetical dispersionless metamaterial slab structure, but unfortunately, it is not clear how this can be practically realized.

One disadvantage of the metamaterial slab structure compared with the PRS structure is that the thickness of the metamaterial slab antenna is much larger than the thickness of the PRS antenna, by a factor of $1/\sqrt{\varepsilon_r}$, where $\varepsilon_r \ll 1$ is the (small) relative permittivity of the artificial slab. It is possible that the metamaterial slab antenna is advantageous over the PRS antenna for some applications, but this remains to be explored.

IV. DIRECTIVE BEAMING AT OPTICAL FREQUENCIES

A. Introduction

Recently, there have been interesting developments within the optics community related to the optical transmission of light through a subwavelength hole in a metal film such as silver or gold. The percentage of power that gets transmitted through a small subwavelength hole is normally quite small. However, it was discovered that when the entrance face of the film (the face that is illuminated by the light) is patterned by a periodic array of grooves, the amount of light that is transmitted through the hole to the exit face of the film can be greatly increased, by orders of magnitude, by using an appropriately optimized periodic patterning [37]–[41]. This effect is referred to as the *enhanced transmission of light*. The enhanced transmission effect also occurs with periodic arrays of holes [42]–[46], and has been realized not only at optical frequencies but at lower microwave and millimeter-wave frequencies [47]–[53]. In this paper, however, the focus is on the single hole.

It was also discovered that when the exit (radiating) face of the film has a periodic array of grooves, the beam that is radiated by the hole can be made quite narrow [54]–[57]. This effect is referred to as the *directive beaming of light*. In this situation, the periodic set of grooves on the exit face acts to focus the radiation from the radiating aperture into a narrow beam. The aperture on the exit face in this case is simply acting as a source, and thus the directive-beaming effect is expected to occur with a general source placed on the exit face of the film.

The enhanced-transmission and directive-beaming effects that occur at optical frequencies when a hole is surrounded by an optimized periodic structure are particularly pronounced when the metal film is silver or gold. These metals behave as plasmonic materials at optical frequencies, meaning that they have a relative permittivity with a negative real part. For ideal lossless plasmonic metals, the permittivity is described approximately by the lossless Drude equation of (44), where f_p is termed the plasmon resonance frequency [58]. Realistic metals have loss at optical frequencies, but for metals such as silver and gold, the loss may be relatively mild. For these metals, operating close to, but below, the plasmon resonance frequency will result in a relative permittivity with a negative real part.

It is well known that because of the negative permittivity at optical frequencies, a metal/air interface will support the propagation of a TM_z surface wave (where z is the direction normal to the interface). This surface wave is termed a "surface plasmon" [58], but is referred to here as a "plasmon surface wave" to emphasize the physical surface-wave characteristics. For an interface between air and a half-space of material with a relative

permittivity $\varepsilon_r = \varepsilon_r' - j\varepsilon_r''$, with $\varepsilon_r' < 0$, an exact solution for the wavenumber of the plasmon surface wave is

$$k_p = k_0 \sqrt{\frac{\varepsilon_r}{1 + \varepsilon_r}}. \qquad (49)$$

For a lossless plasmonic material $(\varepsilon_r'' = 0)$ the wavenumber k_p is real and larger than k_0 when $\varepsilon_r' < -1$. The plasmon is thus a slow wave (not a leaky wave) and hence does not radiate. The plasmon has fields that decay exponentially both in the air region and the metal region. The fields decay in the air region because $k_p > k_0$, and they decay inside the metal region because of the negative value of ε_r'. Because of the exponential decay inside the metal region, the plasmon is hardly affected by replacing the semi-infinite metal region with a finite-thickness metal film, as long as the film thickness is at least several penetration depths. (For thinner film, one must account for the film thickness, in which case the wavenumber of the plasmon surface wave must be determined numerically.)

It was realized that the plasmon is responsible for the enhanced-transmission and the directive-beaming phenomena at optical frequencies, and theories were proposed to explain these phenomena in terms of plasmons [37]–[46], [54]–[57]. It was then discovered that these effects could also be explained in terms of the excitation of a leaky mode on the film [59]. This explanation provides much physical insight, and allows for a simple design formula to optimize the structure. The leaky-wave analysis also allows for a simple calculation, based on the attenuation constant of the leaky mode, for the transverse dimensions of the film needed to fully capture the desired effects. (For example, the dimensions could be chosen so that 90% of the power carried in the leaky mode has been radiated when the mode reaches the outer perimeter of the structure.) The leaky-wave point of view will be summarized here.

The directive-beaming and enhanced-transmission effects are related by reciprocity [60]. The discussion here will focus on the directive-beaming phenomenon, and will assume a 1-D periodic structure (periodic in one transverse direction and uniform in the other) for simplicity. The structure under consideration is shown in Fig. 3. An optical beam (assumed to be a plane wave) is incident on a silver film of thickness W. It is assumed that the electric field of the plane wave is polarized in the x-direction, which is perpendicular to the grooves. On the exit face there is a periodic set of grooves, with a periodic spacing d in the x-direction. Each groove has a width a and a depth h. The structure is assumed to be uniform in the y-direction and infinite in both the x- and y-directions. Both lossless and realistic lossy silver films will be considered. The relative permittivity of the lossless silver film is modeled with the lossless Drude equation (44), while for the lossy case the Lorenz–Drude model is used [58].
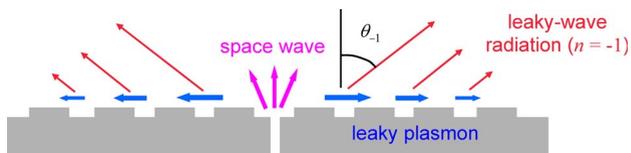

Fig. 21. *A sketch showing the physics of the radiation from the hole on the exit face of the film for the structure of Fig. 3. The hole produces a direct space-wave radiation and also launches a plasmon surface wave that becomes a leaky mode due to radiation from the $n = -1$ space harmonic.*

B. Physics of Directive Beaming

Fig. 21 illustrates the principle of the directive-beaming effect. On the exit face, the aperture acts as a source (which is fairly well approximated as a magnetic line source). This source radiates into space, producing a direct "space-wave" radiation. The space-wave radiation is essentially the same with or without the grooves. In addition to the space-wave radiation, the source launches a plasmon surface wave that propagates away from the source in both directions. Without the grooves, the plasmon would be a nonradiating surface wave. However, due to the periodic set of grooves, the guided plasmon surface-wave mode that propagates on the periodic structure has an infinite set of space harmonics (Floquet waves) [61], with the nth space harmonic having a wavenumber

$$k_{x,n} = k_{x,0} + \frac{2\pi n}{d} = \beta_n - j\alpha. \qquad (50)$$

The wavenumber $k_{x,0}$ is the fundamental wavenumber of the guided plasmon mode, and is slightly different from k_p due to the perturbing effect of the grooves. The field of the guided mode excited by the source has the form (illustrating for the H_y component)

$$H_y(x) = \sum_{n=-\infty}^{\infty} A_n e^{-jk_{x,n}|x|}. \qquad (51)$$

By properly choosing the period d, the phase constant $\beta_{-1} = \text{Re}(k_{x,-1})$ of the $n = -1$ space harmonic can be made to lie within the fast-wave region, so that $-k_0 < \beta_{-1} < k_0$. This space harmonic is then a radiating wave, radiating a pair of beams at an angle $\pm\theta_{-1}$ from the z-axis, where $\beta_{-1} = k_0 \sin \theta_{-1}$. Because of the radiation from the $n = -1$ harmonic, the overall guided mode on the periodic structure is actually a leaky plasmon mode with an attenuation (leakage) constant α due to the radiation (leakage). This attenuation constant will exist even for a lossless film. If the film is lossy, the total attenuation constant will be the sum of the leakage attenuation

constant and the attenuation constant due to material loss. Note that all space harmonics in (50) have the same attenuation constant, and hence the attenuation constant characterizes the overall leaky mode on the structure. The leaky plasmon mode on the corrugated silver film radiates in exactly the same manner as does a leaky mode on a periodic type of leaky-wave antenna [62], [63], where radiation also occurs by virtue of a radiating $n = -1$ space harmonic. This is in contrast to the type of leaky mode that exists on a uniform guiding structure or a quasi-uniform guiding structure [62], [63]. In the latter case, the structure is periodic but radiation occurs from the fundamental $(n = 0)$ space harmonic. The leaky-wave antennas discussed in the previous sections were in these categories. The reader is referred to [61], [64], and [65] for a further discussion of the basic physics of leaky modes.

If the period d is adjusted, the two beams pointing at $\pm\theta_{-1}$ will merge together to form a single beam pointing at broadside. From an analysis of periodic leaky-wave antennas, it has been established that the optimum broadside beam with maximum power density radiated at broadside is produced when the condition

$$|\beta_{-1}| = \alpha \qquad (52)$$

is satisfied [66]. When this condition is satisfied, the two beams (from the forward and backward traveling leaky modes) merge together into a single beam with an optimum radiated power density at broadside. Equation (52) provides a convenient method for optimizing the structure. One can analyze the propagation of the leaky mode on the structure and determine the necessary period d, for a given groove depth h and width a, to satisfy (52).

Knowing the attenuation constant α also gives a simple way of estimating the length of the structure in the x-direction that is necessary to achieve the desired beaming effect. Following standard leaky-wave antenna design rules, the length could be (somewhat arbitrarily) chosen so that 90% of the power in the leaky mode has been radiated by the time the mode reaches the ends of the structure. This yields the simple design equation
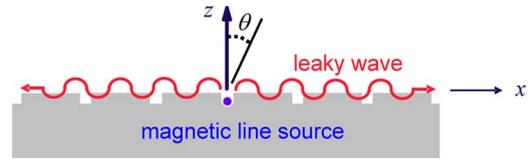
$$e^{-2\alpha L} = 0.1 \qquad (53)$$

Fig. 22. *The model that was used in the calculations, in which the aperture on the exit face of the film has been replaced with a magnetic line source. The dimensions of the structure are as labeled in Fig. 3. (Figure is from [59].)*

where L is the half-length of the structure, measured from source to end.

C. Results

Results for the structure of Fig. 3 are shown for four cases; the groove depth is either 40 or 30 nm, and results are shown for both a lossless silver film and a realistic lossy film (where the loss is accounted for by using a Lorenz–Drude model with parameters from [58]). Table 5 summarizes the four cases, and shows the wavelength used for each case. The structure is excited by an infinite magnetic line source in the y-direction on top of the structure, modeling the aperture [59]. The model used in the calculation is shown in Fig. 22. For each of the four cases the wavelength was chosen to maximize the power density radiated at broadside $(\theta = 0)$.

Fig. 23 shows the aperture field H_y along the aperture, calculated by using a numerical finite-difference time-domain (FDTD) method together with the array scanning method (ASM) [59]. The ASM-FDTD technique allows for an efficient calculation of the fields of an infinite periodic structure when excited by a single (nonperiodic) source, as it requires the numerical meshing of only a single unit cell. The field is sampled at the center of each groove, for the cases where the groove depth is 40 nm [Fig. 23(a)] and 30 nm [Fig. 23(b)]. Results are shown on each plot for a lossless silver film and a realistic lossy film. Also superimposed with each curve is a simple exponential function, which appears as a straight line on the log scale. The straight line is a best-fit solution to the sampled field, and is used to extract the attenuation constant α of the leaky mode. The phase constant β_{-1} is similarly found by curve fitting the phase of the sampled field. Fig. 23 shows that even for the lossless film, the field along the interface

Table 5 Optimized Wavelengths and Numerically Extracted Wavenumbers

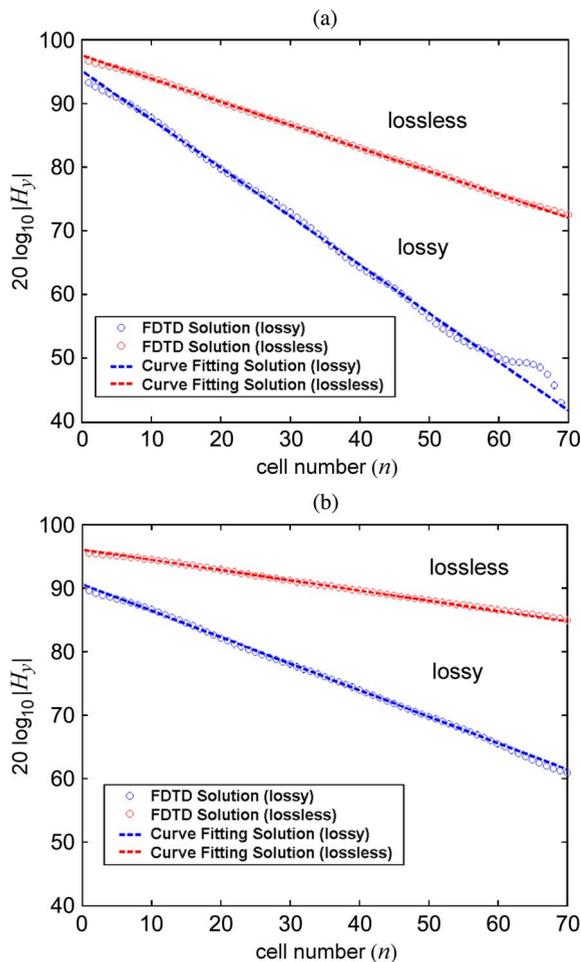| h (nm)	Lossy	Model	Optimized wavelength (nm)	Phase and Attenuation Constants ($\times 10^{-3}$)	
40	Yes	Lorenz-Drude	698.9	$\beta_{-1}/k_0 = 18.6$	$\alpha/k_0 = 15.0$
40	No	Drude	697.2	$\beta_{-1}/k_0 = 7.94$	$\alpha/k_0 = 7.03$
30	Yes	Lorenz-Drude	686.1	$\beta_{-1}/k_0 = 10.1$	$\alpha/k_0 = 8.05$
30	No	Drude	677.5	$\beta_{-1}/k_0 = 2.93$	$\alpha/k_0 = 2.97$

Fig. 23. *A plot of the aperture field H_y versus the distance from the source, for the structure of Fig. 22, excited by a magnetic line source on top of the film, which serves as a model for the radiating aperture on the exit face. The film is either lossless or modeled with realistic losses. (a) The groove depth is $h = 40$ nm. (b) The groove depth is $h = 30$ nm. The wavelength of operation is given in Table 5. The other parameters are: $d = 650$ nm, $W = 350$ nm, $a = 40$ nm. (Figure is from [59].)*

decays exponentially, as expected for a leaky mode. For the lossy film the attenuation constant is larger, as expected, since the leakage attenuation constant and the loss attenuation constant are now both contributing to the total attenuation constant. It is also seen that the leakage attenuation constant is smaller for the case of the shallower grooves (30 nm). This is because shallower grooves present less of a perturbation from the smooth film, and hence the amplitude of the $n = -1$ space harmonic is less. Table 5 shows the complex wavenumber $k_{x,-1} = \beta_{-1} - j\alpha$ that is determined numerically from the curve fitting of the sampled aperture field. As expected, at the optimum wavelength $\beta_{-1} \approx \alpha$.

The radiation pattern of the magnetic line source on the grooved film is then calculated by using the complex

wavenumber of the leaky mode along with a simple array factor calculation, as is commonly done in antenna theory [22]. Since all of the space harmonics in (51) have the same phase shift and amplitude change in going from one unit cell (groove) to the next, the pattern can be calculated by using only the dominant $n = 0$ harmonic. The normalized H_y field $\psi(x)$ is sampled at x_q, the center of the qth cell, where $x_q = (q - 1/2)d$ for $q > 0$ and $x_q = (q + 1/2)d$ for $q < 0$. The sampled field is determined directly from the wavenumber $k_{x,0}$ as

$$\psi_q = \psi(x_q) = e^{-jk_{x,0}d(q-1/2)}, \qquad q > 0$$
$$\psi_q = \psi(x_q) = e^{+jk_{x,0}d(q+1/2)}, \qquad q < 0. \qquad (54)$$

The normalized far-field pattern is then given by the antenna array factor AF as

$$AF(\theta) = \sum_{q=1}^{\infty} \psi_q e^{jk_0 \sin(\theta)(qd-d/2)} + \sum_{q=-1}^{-\infty} \psi_q e^{jk_0 \sin(\theta)(qd+d/2)}$$

$$(55)$$

which may be evaluated in closed form by summing the geometric series [59]. Fig. 24 shows a comparison of the exact radiation pattern calculated numerically with the simple array-factor calculation of (55), for the 40- and 30-nm groove depths in the lossless case. For each groove depth the agreement near the beam peak is good, with better agreement in the 30-nm case. This is expected, since the leaky mode has a smaller attenuation constant for the shallower grooves, and is thus a more dominant part of the total aperture field since it will propagate out to larger distances from the source.

A leaky-mode analysis of a realistic 2-D grooved structure is not available at this time. However, in [60], a hypothetical 2-D structure was analyzed. The structure, shown in Fig. 25, consists of a 2-D periodic array of perfectly conducting patches on top of a silver film. The structure is hypothetical, since perfect conductors do not exist at optical frequencies. However, the patches serve as a simplistic surrogate for realistic grooves, so that the structure can be analyzed in a fairly simple manner [60]. The structure is excited by a y-directed magnetic dipole on top of the structure, modeling the aperture. Fig. 26 shows a comparison of the E-plane (xz) pattern due to the periodic array of patches (responsible for the narrow beam) and the pattern of the leaky mode, calculated using the 1-D array factor in (55). It is seen that the agreement is very good near the beam peak, confirming that the leaky mode is responsible for the directive-beaming effect.
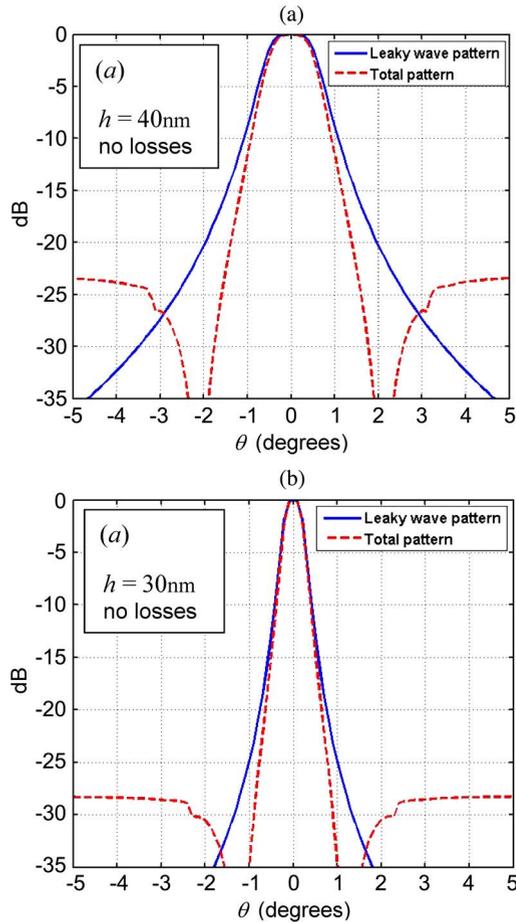
Fig. 24. *A comparison of* H*-plane far-field patterns for the structure of Fig. 23, for the case of a lossless film. (a) The groove depth is h = 40 nm. (b) The groove depth is h = 30 nm. The other dimensions and operating wavelengths are as listed in Fig. 23. (Figure is from [59].)*

Although the directive-beaming effect described above using plasmonics has been illustrated at optical frequencies, the effect may be extended down in frequency into the THz region, with important applications to quantum-cascade lasers [67], [68].
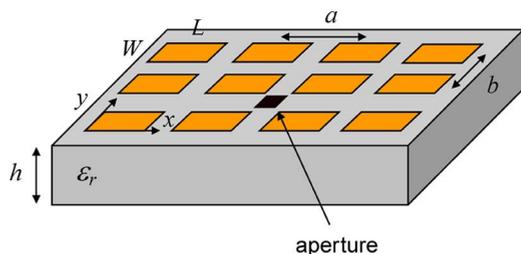

Fig. 25. *A silver film with a 2-D periodic array of hypothetical perfectly conducting rectangular patches on the surface. The patches serve as a surrogate for a more realistic type of perturbation such as grooves in the film. (Figure is adapted from [60].)*
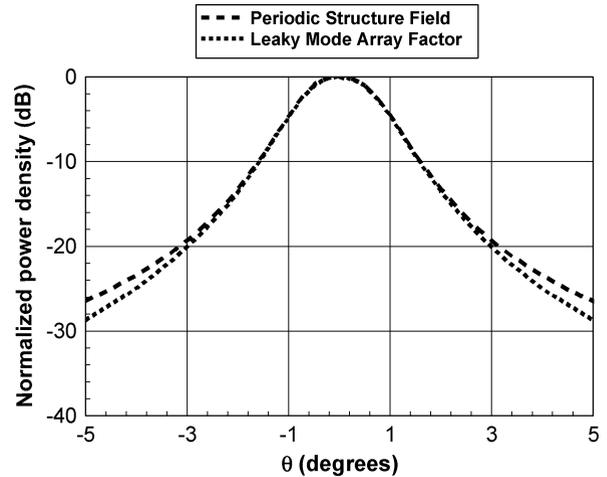

Fig. 26. *A comparison of* E*-plane radiation patterns for the structure of Fig. 25. The pattern produced by the periodic array of patches is compared with the pattern of the leaky-mode array factor. The film thickness is 300 nm. The film is lossless with a relative permittivity of $\varepsilon_r = -4.5$. The dimensions of the patches are L = 140 nm, W = 50 nm. The periodic spacings in the x- and y-directions are a = 377 nm and b = 90 nm. The operating wavelength is 400 nm, corresponding to an optimum broadside beam. The structure is excited by a y-directed magnetic dipole on top of the film at the aperture location. (Figure is from [60].)*

V. CONCLUSION

In this review paper, the subject of directive beaming from planar structures at microwave and optical frequencies has been reviewed, with the aim of explaining how the various phenomena are due to the excitation of one or more leaky modes on the structure. Three different types of directive-beaming structures were discussed. The first two of them were antenna structures, where the objective is to produce a narrow beam of radiation. The third structure exhibits the optical phenomenon known as directive beaming from a subwavelength aperture.

The first structure considered is the Fabry–Pérot cavity type of antenna, which uses a PRS over a grounded substrate. The structure is excited by a simple source inside the cavity. When optimized properly, a narrow pencil beam at broadside or a conical beam that is focused at a scan angle may be produced. Design formulas for this type of antenna were presented, and the operation of the structure as a leaky-wave antenna was discussed. Results were shown for various types of PRS surfaces, in order to examine practical radiation characteristics.

The second structure considered is the metamaterial-slab antenna that consists of an artificial low-permittivity slab over a ground plane. This type of structure can be realized by using a wire-medium slab and operating at a frequency above but close to the plasma resonance frequency of the wire medium. This structure produces a narrow beam of radiation at broadside when the relative

permittivity of the slab becomes small. Although ray optics provides a partial explanation of the narrow-beam radiation from this structure, a complete explanation is provided by examining the leaky mode that is excited by the source and propagates on the low-permittivity grounded slab.

The third structure that was considered is one that exhibits the optical phenomenon of directive beaming of light from a subwavelength aperture in a plasmonic metal film such as silver. The metal has a negative permittivity at optical frequencies, and therefore supports a plasmon type of surface wave. The beam radiated by the aperture can be made directive by surrounding the aperture with an optimized periodic array of grooves on the film. It was shown here that the directive beaming is due to a leaky mode that is the evolution of the nonradiating plasmon mode on the smooth silver film when the grooves are added.

In all cases, it was observed that leaky modes play a key role in the phenomena, and provide physical insight into the operation of the structure. An understanding of the leaky-mode properties allows for a more complete understanding of how to optimize the structure and also how to terminate it in order to have a practical finite-size structure with the desired characteristics. ∎

REFERENCES

[1] G. von Trentini, "Partially reflecting sheet arrays," *IEEE Trans. Antennas Propag.*, vol. AP-4, no. 4, pp. 666–671, Oct. 1956.

[2] D. R. Jackson and N. G. Alexopoulos, "Gain enhancement methods for printed circuit antennas," *IEEE Trans. Antennas Propag.*, vol. AP-33, no. 9, pp. 976–987, Sep. 1985.

[3] D. R. Jackson and A. A. Oliner, "A leaky-wave analysis of the high-gain printed antenna configuration," *IEEE Trans. Antennas Propag.*, vol. AP-36, no. 7, pp. 905–910, Jul. 1988.

[4] H. Y. Yang and N. G. Alexopoulos, "Gain enhancement methods for printed circuit antennas through multiple superstrates," *IEEE Trans. Antennas Propag.*, vol. AP-35, no. 7, pp. 860–863, Jul. 1987.

[5] D. R. Jackson, A. A. Oliner, and A. Ip, "Leaky-wave propagation and radiation for a narrow-beam multiple-layer dielectric structure," *IEEE Trans. Antennas Propag.*, vol. 41, no. 3, pp. 344–348, Mar. 1993.

[6] T. Akalin, J. Danglot, O. Vanbésien, and D. Lippens, "A highly directive dipole antenna embedded in a Fabry-Pérot type cavity," *IEEE Microw. Wireless Compon. Lett.*, vol. 12, no. 2, pp. 48–50, Feb. 2002.

[7] A. P. Feresidis and J. C. Vardaxoglou, "High gain planar antenna using optimised partially reflective surfaces," *Inst. Electr. Eng. Proc.—Microw. Antennas Propag.*, vol. 148, pp. 345–350, Dec. 2001.

[8] R. Gardelli, M. Albani, and F. Capolino, "Array thinning by using antennas in a Fabry-Perot cavity for gain enhancement," *IEEE Trans. Antennas Propag.*, vol. 54, no. 7, pp. 1979–1990, Jul. 2006.

[9] T. Zhao, D. R. Jackson, J. T. Williams, H. Y. Yang, and A. A. Oliner, "2-D periodic leaky-wave antennas: Part I: Metal patch design," *IEEE Trans. Antennas Propag.*, vol. 53, no. 11, pp. 3505–3515, Nov. 2005.

[10] T. Zhao, D. R. Jackson, and J. T. Williams, "2-D periodic leaky-wave antennas—Part II: Slot design," *IEEE Trans. Antennas Propag.*, vol. 53, no. 11, pp. 3515–3524, Nov. 2005.

[11] H. Boutayeb, K. Mahdjoubi, A.-C. Tarot, and T. A. Denidni, "Directivity of an antenna embedded inside a Fabry-Pérot cavity: Analysis and design," *Microw. Opt. Technol. Lett.*, vol. 48, pp. 12–17, Jan. 2006.

[12] N. Guèrin, S. Enoch, G. Tayeb, P. Sabouroux, P. Vincent, and H. Legay, "A metallic Fabry-Pérot directive antenna," *IEEE Trans. Antennas Propag.*, vol. 54, no. 1, pp. 220–224, Jan. 2006.

[13] T. Zhao, D. R. Jackson, and J. T. Williams, "General formulas for 2D leaky wave antennas," *IEEE Trans. Antennas Propag.*, vol. 53, no. 11, pp. 3525–3533, Nov. 2005.

[14] Y. J. Lee, J. Yeo, R. Mittra, and W. S. Park, "Application of electromagnetic bandgap (EBG) superstrates with controllable defects for a class of patch antennas as spatial angular filters," *IEEE Trans. Antennas Propag.*, vol. 53, no. 1, pp. 224–235, Jan. 2005.

[15] M. Thévenot, C. Cheype, A. Reineix, and B. Jecko, "Directive photonic bandgap antennas," *IEEE Trans. Microw. Theory Tech.*, vol. 47, no. 11, pp. 2115–2122, Nov. 1999.

[16] B. Temelkuran, M. Bayindir, E. Ozbay, R. Biswas, M. M. Sigalas, G. Tuttle, and K. M. Ho, "Photonic crystal-based resonant antenna with a very high directivity," *J. Appl. Phys.*, vol. 87, pp. 603–605, 2000.

[17] K. C. Gupta, "Narrow-beam antennas using an artificial dielectric medium with permittivity less than unity," *Electron. Lett.*, vol. 7, pp. 16–18, Jan. 1971.

[18] I. J. Bahl and K. C. Gupta, "A leaky-wave antenna using an artificial dielectric medium," *IEEE Trans. Antennas Propag.*, vol. 22, no. 1, pp. 119–122, Jan. 1974.

[19] S. Enoch, G. Tayeb, P. Sabouroux, N. Guérin, and P. Vincent, "A metamaterial for directive emission," *Phys. Rev. Lett.*, vol. 89, pp. 213902-1–213902-4, Nov. 2002.

[20] R. F. Harrington, *Time Harmonic Electromagnetic Fields*. Piscataway, NJ: Wiley/IEEE Press, 2001.

[21] T. Zhao, D. R. Jackson, J. T. Williams, and A. A. Oliner, "Simple CAD model for a dielectric leaky-wave antenna," *IEEE Antennas Wireless Propag. Lett.*, vol. 3, pp. 243–345, Dec. 2004.

[22] C. A. Balanis, *Antenna Theory: Analysis and Design*, 3rd ed. New York: Wiley, 2005.

[23] N. Marcuvitz, *Waveguide Handbook*. Stevenage, U.K.: Peter Peregrinus, 1986.

[24] G. Lovat, P. Burghignoli, and D. R. Jackson, "Fundamental properties and optimization of broadside radiation from uniform leaky-wave antennas," *IEEE Trans. Antennas Propag.*, vol. 54, no. 5, pp. 1442–1452, May 2006.

[25] H. Ostner, J. Detlefsen, D. R. Jackson, and E. Schmidhammer, "Radiation from dielectric leaky-wave antennas with circular and rectangular apertures," *Electromagnetics*, vol. 17, no. 5, pp. 505–535, Sep.–Oct. 1997.

[26] T. Zhao, "Analysis and design of 2D periodic leaky wave antennas using metal patches or slots," Ph.D. dissertation, Dept. Electr. Comput. Eng., Univ. Houston, Houston, TX, 2003.

[27] P. Burghignoli, G. Lovat, F. Capolino, D. R. Jackson, and D. R. Wilton, "Highly polarized, directive radiation from a Fabry-Pérot cavity leaky-wave antenna based on a metal strip grating," *IEEE Trans. Antennas Propag*, vol. 58, no. 12, pp. 3873–3883, Dec. 2010.

[28] J. Brown, "Artificial dielectrics having refractive indices less than unity," *Proc. Inst. Electr. Eng.*, vol. 100, pp. 51–62, May 1953.

[29] R. N. Bracewell, "Analogues of an ionized medium: Applications to the ionosphere," *Wireless Eng.*, vol. 31, pp. 320–326, Dec. 1954.

[30] W. Rotman, "Plasma simulation by artificial dielectrics and parallel plate media," *IRE Trans. Antennas Propag.*, vol. AP-10, no. 1, pp. 82–95, Jan. 1962.

[31] S. Ramo, J. R. Whinnery, and T. Van Duzer, *Fields and Waves in Communicational Electronics,* 3rd ed. New York: Wiley, 1994.

[32] P. A. Belov, R. Marqués, S. I. Maslovski, I. S. Nefedov, M. Silveirinha, C. R. Simovski, and S. A. Tretyakov, "Strong spatial dispersion in wire media in the very large wavelength limit," *Phys. Rev. B*, vol. 67, pp. 113103-1–113103-4, 2003.

[33] G. Lovat, P. Burghignoli, F. Capolino, and D. R. Jackson, "High directivity in low-permittivity metamaterial slabs: Ray-optic vs. leaky-wave models," *Microw. Opt. Technol. Lett.*, vol. 48, *Special Issue on Metamaterials and Special Materials for Electromagnetic Applications and Telecommunications*, no. 12, pp. 2542–2548, Dec. 2006.

[34] G. Lovat, P. Burghignoli, F. Capolino, D. R. Jackson, and D. R. Wilton, "Analysis of directive radiation from a line source in a metamaterial slab with low permittivity," *IEEE Trans. Antennas Propag.*, vol. 54, no. 3, pp. 1017–1030, Mar. 2006.

[35] P. Burghignoli, G. Lovat, F. Capolino, D. R. Jackson, and D. R. Wilton, "Directive leaky-wave radiation from a dipole source in a wire medium slab," *IEEE Trans. Antennas Propag*, vol. 56, no. 5, pp. 1329–1339, May 2008.

[36] G. Lovat, P. Burghignoli, F. Capolino, and D. R. Jackson, "Highly-directive planar leaky-wave antennas: A comparison between metamaterial-based and conventional designs," *Proc. Eur. Microw. Assoc.*, vol. 2, pp. 12–21, Mar. 2006.

[37] T. Thio, K. M. Pellerin, R. A. Linke, H. J. Lezec, and T. W. Ebbesen, "Enhanced light transmission through a single subwavelength aperture," *Opt. Lett.*, vol. 26, pp. 1972–1974, 2001.

[38] T. Thio, H. J. Lezec, T. W. Ebbesen, K. M. Pellerin, G. D. Lewen, A. Nahata, and R. A. Linke, "Giant optical transmission of sub-wavelength apertures: Physics and applications," *Nanotechnology*, vol. 13, no. 3, pp. 429–432, 2002.

[39] F. J. Garcia-Vidal, H. J. Lezec, T. W. Ebbesen, and L. Martín-Moreno, "Multiple paths to enhance optical transmission through a single subwavelength slit," *Phys. Rev. Lett.*, vol. 90, no. 21, 213901, 2003.

[40] A. Degiron and T. W. Ebbesen, "Analysis of the transmission process through single apertures surrounded by periodic corrugations," *Opt. Exp.*, vol. 12, pp. 3694–3700, 2004.

[41] H. Caglayan, I. Bulu, and E. Ozbay, "Extraordinary grating-coupled microwave transmission through a subwavelength annular aperture," *Opt. Exp.*, vol. 13, pp. 1666–1671, 2005.

[42] T. W. Ebbesen, H. J. Lezec, H. F. Ghaemi, T. Thio, and P. A. Wolff, "Extraordinary transmission through sub-wavelength hole arrays," *Nature*, vol. 391, pp. 667–669, 1998.

[43] T. Thio, H. F. Ghaemi, H. J. Lezec, P. A. Wolff, and T. W. Ebbesen, "Surface plasmon-enhanced transmission through hole arrays in Cr films," *J. Opt. Soc. Amer. B*, vol. 16, pp. 1743–1748, 1999.

[44] L. Martín-Moreno, F. J. García-Vidal, H. J. Lezec, K. M. Pellerin, T. Thio, J. B. Pendry, and T. W. Ebbesen, "Theory of extraordinary optical transmission through subwavelength hole arrays," *Phys. Rev. Lett.*, vol. 86, pp. 1114–1117, 2001.

[45] S. Enoch, E. Popov, M. Nevière, and R. Reinisch, "Enhanced light transmission by hole arrays," *J. Opt. A, Pure Appl. Opt.*, vol. 4, pp. S83–S87, 2002.

[46] C. Genet and T. W. Ebbesen, "Light in tiny holes," *Nature*, vol. 445, pp. 39–46, 2007.

[47] J. B. Pendry, L. Martín-Moreno, and F. J. García-Vidal, "Mimicking surface plasmons with structured surfaces," *Science*, vol. 305, pp. 847–848, 2004.

[48] M. Beruete, M. Sorolla, I. Campillo, J. S. Dolado, L. Martín-Moreno, J. Bravo-Abad, and F. J. García-Vidal, "Enhanced millimeter wave transmission through quasioptical subwavelength perforated plates," *IEEE Trans. Antennas Propag.*, vol. 53, no. 6, pp. 1897–1903, Jun. 2005.

[49] M. Beruete, M. Sorolla, M. N. Cia, F. Falcone, I. Campillo, and V. Lomakin, "Extraordinary transmission and left-handed propagation

in miniaturized stacks of doubly periodic subwavelength hole arrays," *Opt. Exp.*, vol. 15, no. 3, pp. 1107–1114, 2007.

[50] V. Lomakin, N. W. Chen, S. Q. Li, and E. Michielssen, "Enhanced transmission through two-period arrays of sub-wavelength holes," *IEEE Microw. Wireless Compon. Lett.*, vol. 14, no. 7, pp. 355–357, Jul. 2004.

[51] V. Lomakin and E. Michielssen, "Enhanced transmission through metallic plates perforated by arrays of subwavelength holes and sandwiched in between dielectric slabs," *Phys. Rev. B*, vol. 71, no. 23, pp. 235117-1–235117-10, 2005.

[52] V. Lomakin and E. Michielssen, "Beam transmission through periodic sub-wavelength hole structures," *IEEE Trans. Antennas Propag.*, vol. 55, no. 6, pp. 1564–1581, Jun. 2007.

[53] V. Lomakin, S. Li, and E. Michielssen, "Transmission through and wave guidance on metal plates perforated by periodic arrays of through-holes of subwavelength coaxial cross-section," *Microw. Opt. Technol. Lett.*, vol. 49, no. 7, pp. 1554–1558, 2007.

[54] H. J. Lezec, A. Degiron, E. Devaux, R. A. Linke, L. Martin-Moreno, F. J. Garcia-Vidal, and T. W. Ebbesen, "Beaming light from a subwavelength aperture," *Science*, vol. 297, pp. 820–822, 2002.

[55] L. Martin-Moreno, F. J. Garcia-Vidal, H. J. Lezec, A. Degiron, and T. W. Ebbesen, "Theory of highly directive emission from a single subwavelength aperture surrounded by surface corrugations," *Phys. Rev. Lett.*, vol. 90, no. 16, 167401, 2003.

[56] F. J. Garcia-Vidal, L. Martin-Moreno, H. J. Lezec, and T. W. Ebbesen, "Focusing light with a single subwavelength aperture flanked by surface corrugations," *Appl. Phys. Lett.*, vol. 83, pp. 4500–4502, 2003.

[57] H. Caglayan, I. Bulu, and E. Ozbay, "Plasmonic structures with extraordinary transmission and highly directional beaming properties," *IEEE Microw. Opt. Technol. Lett.*, vol. 48, no. 12, pp. 2491–2496, 2006.

[58] A. D. Rakic, A. B. Djurisic, J. M. Elazar, and M. L. Majewski, "Optical properties

of metallic films for vertical-cavity optoelectronic devices," *Appl. Opt.*, vol. 37, no. 22, pp. 5271–5283, 1998.

[59] D. R. Jackson, J. Chen, R. Qiang, F. Capolino, and A. A. Oliner, "The role of leaky plasmon waves in the directive beaming of light through a subwavelength aperture," *Opt. Exp.*, vol. 16, no. 26, pp. 21271–21281, Dec. 22, 2008.

[60] D. R. Jackson, A. A. Oliner, T. Zhao, and J. T. Williams, "The beaming of light at broadside through a subwavelength hole: Leaky-wave model and open stopband effect," *Radio Sci.*, vol. 40, pp. 1–12, 2005.

[61] A. Hessel, "General characteristics of traveling-wave antennas," in *Antenna Theory*, R. E. Collin and F. J. Zucker, Eds. New York: McGraw-Hill, 1969, pt. 2, ch. 19.

[62] A. A. Oliner and D. R. Jackson, "Leaky-wave antennas," in *Antenna Engineering Handbook*, J. L. Volakis, Ed. New York: McGraw Hill, 2007.

[63] D. R. Jackson and A. A. Oliner, "Leaky-wave antennas," in *Modern Antenna Handbook*, C. Balanis, Ed. New York: Wiley, 2008.

[64] T. Tamir and A. A. Oliner, "Guided complex waves, Part I," *Proc. Inst. Electr. Eng.*, vol. 110, pp. 310–324, Feb. 1963.

[65] T. Tamir and A. A. Oliner, "Guided complex waves, part II," *Proc. Inst. Electr. Eng.*, vol. 110, pp. 325–334, Feb. 1963.

[66] P. Burghignoli, G. Lovat, and D. R. Jackson, "Analysis and optimization of leaky-wave radiation at broadside from a class of 1-D periodic structures," *IEEE Trans. Antennas Propag.*, vol. 54, no. 9, pp. 2593–2604, Sep. 2006.

[67] N. Yu, R. Blanchard, J. Fan, Q. J. Wang, C. Pflügl, L. Diehl, T. Edamura, M. Yamanishi, H. Kan, and F. Capasso, "Quantum cascade lasers with integrated plasmonic antenna-array collimators," *Opt. Exp.*, vol. 16, no. 24, pp. 19447–19461, 2008.

[68] N. Yu and F. Capasso, "Wavefront engineering for mid-infrared and terahertz quantum cascade lasers," *J. Opt. Soc. Amer. B*, vol. 27, no. 11, pp. B18–B35, 2010.

ABOUT THE AUTHORS

David R. Jackson (Fellow, IEEE) was born in St. Louis, MO, on March 28, 1957. He received the B.S.E.E. and M.S.E.E. degrees from the University of Missouri, Columbia, in 1979 and 1981, respectively, and the Ph.D. degree in electrical engineering from the University of California, Los Angeles, in 1985.

From 1985 to 1991, he was an Assistant Professor at the Department of Electrical and Computer Engineering, University of Houston, Houston, TX. From 1991 to 1998, he was an Associate Professor in the same department, and since 1998, he has been a Professor in this department. His present research interests include microstrip antennas and circuits, leaky-wave antennas, leakage and radiation effects in microwave integrated circuits, periodic structures, and electromagnetic compatibility and interference.

Dr. Jackson is presently serving as the Chair of the Distinguished Lecturer Committee of the IEEE Antennas and Propagation Society (AP-S), and as a Member-at-Large for U.S. Commission B of the International Union of Radio Science (URSI). He also serves as the Chair of the Microwave Field Theory (MTT-15) Technical Committee and is on the Editorial Board for the IEEE TRANSACTIONS ON MICROWAVE THEORY AND TECHNIQUES. Previously, he has been the Chair of the Transnational Committee for the IEEE AP-S Society, the Chapter Activities Coordinator for the AP-S Society, a Distinguished Lecturer for the AP-S Society, a member of the AdCom for the AP-S Society, and an Associate Editor for the IEEE TRANSACTIONS ON ANTENNAS AND PROPAGATION. He has also served as the Chair of U.S. Commission B of URSI. He has also served as an Associate Editor for the *Journal Radio Science* and the *International Journal of RF and Microwave Computer-Aided Engineering*.

Paolo Burghignoli (Senior Member, IEEE) was born in Rome, Italy, on February 18, 1973. He received the Laurea degree (*cum laude*) in electronic engineering and the Ph.D. degree in applied electromagnetics from "La Sapienza" University of Rome, Rome, Italy, in 1997 and 2001, respectively.
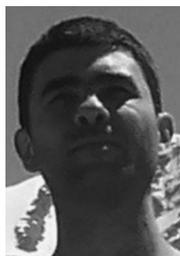
In 1997, he joined the Electronic Engineering Department, "La Sapienza" University of Rome, where he has been an Assistant Professor since November 2010. From January 2004 to July 2004, he was a Visiting Research Assistant Professor at the University of Houston, Houston, TX. His scientific interests include analysis and design of planar leaky-wave antennas, numerical methods for the analysis of passive guiding and radiating microwave structures, periodic structures, and propagation and radiation in metamaterials.

Dr. Burghignoli was the recipient of a 2003 IEEE Microwave Theory and Techniques Society (IEEE MTT-S) Graduate Fellowship, the 2005 Raj Mittra Travel Grant for Junior Researchers presented at the IEEE Antennas and Propagation Society Symposium, Washington, DC, and the 2007 "Giorgio Barzilai" Laurea Prize presented by the former IEEE Central & South Italy Section. He is a coauthor of the "Fast Breaking Papers, October 2007" in electrical engineering and computer science, about metamaterials [paper that had the highest percentage increase in citations in Essential Science Indicators (ESI)].

Giampiero Lovat (Member, IEEE) was born in Rome, Italy, on May 31, 1975. He received the Laurea degree (*cum laude*) in electronic engineering and the Ph.D. degree in applied electromagnetics from "La Sapienza" University of Rome, Rome, Italy, in 2001 and 2005, respectively.

In 2005, he joined the Electrical Engineering Department, "La Sapienza" University of Rome, where he is currently an Assistant Professor at the Astronautical, Electrical, and Energetic Engineering Department. From January 2004 to July 2004, he was a Visiting Scholar at the University of Houston, Houston, Texas. He coauthored the book *Electromagnetic Shielding* (New York: IEEE/Wiley, 2008). His present research interests include leaky waves, general theory and numerical methods for the analysis of periodic structures, and electromagnetic shielding.

Dr. Lovat received a Young Scientist Award from the 2005 International Union of Radio Science (URSI) General Assembly, New Delhi, India. He is a coauthor of "Fast Breaking Papers, October 2007" in electrical engineering and computer science, about metamaterials [paper that had the highest percentage increase in citations in Essential Science Indicators (ESI)].

Filippo Capolino (Senior Member, IEEE) received the Laurea degree (*cum laude*) and the Ph.D. degree in electrical engineering from the University of Florence, Florence, Italy, in 1993 and 1997, respectively.

He is currently employed as an Assistant Professor at the Department of Electrical Engineering and Computer Science, University of California, Irvine, CA. He has been an Assistant Professor at the Department of Information Engineering, University of Siena, Siena, Italy. During 1997–1999, he was a Postdoctoral Fellow with the Department of Aerospace and Mechanical Engineering, Boston University, MA. From 2000 to 2001 and in 2006, he was a Research Assistant Visiting Professor with the Department of Electrical and Computer Engineering, University of Houston, Houston, TX. His research interests include antennas, metamaterials and their applications, sensors in both microwave and optical ranges, wireless systems, chip-integrated antennas. He has been the European Union (EU) Coordinator of the EU Doctoral Programmes on Metamaterials (2004–2009). He is a coauthor of the "Fast Breaking Papers, October 2007" in electrical engineering and computer science, about metamaterials [paper that had the highest percentage increase in citations in Essential Science Indicators (ESI)].

Dr. Capolino received several young and senior scientist travel grants to attend international conferences (IEEE and URSI) and two student and young scientist paper competition awards. He received the R.W. P. King Prize Paper Award from the IEEE Antennas and Propagation Society for the Best Paper of the Year 2000, by an author under 36. In 2002–2008, he has served as an Associate Editor for the IEEE TRANSACTIONS ON ANTENNAS AND PROPAGATION. He is a founder and has been an Editor of the new journal *Metamaterials*, by Elsevier, since 2007. He is the Editor of the *Metamaterials Handbook* (Boca Raton, FL: CRC Press, 2009).

Ji Chen received the B.S. degree from Huazhong University of Science and Technology, Wuhan, China, the M.S. degree from McMaster University, Hamilton, ON, Canada, in 1994, and the Ph.D. degree from the University of Illinois at Urbana-Champaign, Urbana, in 1998, all in electrical engineering.

Currently, he is an Associate Professor at the Department of Electrical and Computer Engineering, University of Houston, Houston, TX. Prior to joining the University of Houston, from 1998 to 2001, he was a Staff Engineer with Motorola Personal Communication Research Laboratories, Chicago, IL.

Dr. Chen has received outstanding teaching award and outstanding junior faculty research award from College of Engineering at University of Houston. His research group also received the best student paper award at the 2005 IEEE Symposium on Electromagnetic Compatibility and the best paper award from the 2008 IEEE Asia-Pacific Microwave Conference.

Donald R. Wilton (Life Fellow, IEEE) was born in Lawton, OK, on October 25, 1942. He received the B.S., M.S., and Ph.D. degrees in electrical engineering from the University of Illinois, Urbana-Champaign, Urbana, in 1964, 1966, and 1970, respectively.

From 1965 to 1968, he was with Hughes Aircraft Co., Fullerton, CA, engaged in the analysis and design of phased array antennas. From 1970 to 1983, he was with the Department of Electrical Engineering, University of Mississippi, and since 1983 he has been Professor of Electrical Engineering at the University of Houston, Houston, TX. From 1978 to 1979, he was a Visiting Professor at Syracuse University, Syracuse, NY. During 2004–2005, he was a Visiting Scholar at the Polytechnic of Turin, Turin, Italy, the Sandia National Laboratories, and the University of Washington. He has authored or coauthored many publications, lectured, and consulted extensively. His primary research interest is in computational electromagnetics.

Dr. Wilton is a member of Commission B of the International Union of Radio Science (URSI), in which he has held various offices including Chair of U.S. Commission B. He received the IEEE Third Millennium Medal. He has served the IEEE Antennas and Propagation Society as an Associate Editor of the IEEE TRANSACTIONS ON ANTENNAS AND PROPAGATION as a Distinguished National Lecturer, and as a member of AdCom.

Arthur A. Oliner (Fellow, IEEE) was born on March 5, 1921, in Shanghai, China. He received the B.A. degree from Brooklyn College, Brooklyn, NY and the Ph.D. degree from Cornell University, Ithaca, NY, both in physics, in 1941 and 1946, respectively.

He joined the Polytechnic Institute of Brooklyn (now Polytechnic University) in 1946, and became Professor in 1957. He then served as Department Head from 1966 to 1974, and was Director of its Microwave Research Institute from 1967 to 1982. He was a Walker-Ames Visiting Professor at the University of Washington, Seattle, in 1964. He has also been a Visiting Professor at the Catholic University, Rio de Janeiro, Brazil, the Tokyo Institute of Technology, Tokyo, Japan, the Central China Institute of Science and Technology, Wuhan, China, and the University of Rome, Rome, Italy. In 2003, the University of Rome (La Sapienza) granted him an Honorary Doctorate, and organized an associated special symposium in his honor. His research has covered a wide variety of topics in the microwave field, including network representations of microwave structures, guided-wave theory with stress on surface waves and leaky waves, waves in plasmas, periodic structure theory, and phased-array antennas. He has made pioneering and fundamental contributions in several of these areas. His interests have also included waveguides for surface acoustic waves and integrated optics, novel leaky-wave antennas for millimeter waves, and leakage effects in microwave integrated circuits. Lately, he has contributed to the topics of metamaterials, and to enhanced propagation through sub-wavelength holes. He is the author of over 300 papers, various book chapters, and the coauthor or coeditor of three books.

Dr. Oliner is a member of the Board of Directors of Merrimac Industries. He is a Fellow of the American Association for the Advancement of Science (AAAS) and the British Institution of Electrical Engineers (IEE), and was a Guggenheim Fellow. He was elected a member of the National Academy of Engineering in 1991. He has received prizes for two of his papers: the IEEE Microwave Prize in 1967 for his work on strip line discontinuities, and the Institution Premium of the British IEE in 1964 for his comprehensive studies of complex wave types guided by interfaces and layers. He was President of the IEEE Microwave Theory and Techniques Society (MTT-S), its first Distinguished Lecturer, and a member of the IEEE Publication Board. He is an Honorary Life Member of MTT-S (one of only six such persons), and in 1982, he received its highest recognition, the Microwave Career Award. A special retrospective session was held in his honor at the International Microwave Symposium (reported in detail in the December 1988 issue of the IEEE Transactions on Microwave Theory and Techniques, pp. 1578–1581). In 1993, he became the first recipient of the Distinguished Educator Award of the MTT-S. He is also a recipient of the IEEE Centennial and Millennium Medals. He is also a past U.S. Chairman of Commissions A and D of the International Union of Radio Science (URSI), a longtime member of and active contributor to Commission B, and a former member of the U.S. National Committee of URSI. In 1990, he was awarded the URSI van der Pol Gold Medal, which is given triennially, for his contributions to leaky waves. In 2000, the IEEE awarded him a second gold medal, the Heinrich Hertz Medal, which is its highest award in the area of electromagnetic waves.